High pressure torsion applied to nickel single crystals

Reinhard Pippan, Martin Hafok

▶ **To cite this version:**

Reinhard Pippan, Martin Hafok. High pressure torsion applied to nickel single crystals. Philosophical Magazine, Taylor & Francis, 2008, 88 (12), pp.1857-1877. 10.1080/14786430802337071 . hal-00513939

HAL Id: hal-00513939

https://hal.archives-ouvertes.fr/hal-00513939

Submitted on 1 Sep 2010

HAL is a multi-disciplinary open access archive for the deposit and dissemination of scientific research documents, whether they are published or not. The documents may come from teaching and research institutions in France or abroad, or from public or private research centers.

L'archive ouverte pluridisciplinaire **HAL**, est destinée au dépôt et à la diffusion de documents scientifiques de niveau recherche, publiés ou non, émanant des établissements d'enseignement et de recherche français ou étrangers, des laboratoires publics ou privés.

High pressure torsion applied to nickel single crystals

Journal:	*Philosophical Magazine & Philosophical Magazine Letters*
Manuscript ID:	TPHM-07-Oct-0295.R2
Journal Selection:	Philosophical Magazine
Date Submitted by the Author:	16-Jun-2008
Complete List of Authors:	Pippan, Reinhard; Erich Schmid Institute of Materials Science Hafok, Martin; Erich Schmid Institute of Materials Science
Keywords:	electron diffraction, plastic deformation
Keywords (user supplied):	nickel, High pressure torsion
Note: The following files were submitted by the author for peer review, but cannot be converted to PDF. You must view these files (e.g. movies) online.	
single-rev-2n.tex	

scholarONE™
Manuscript Central

Philosophical Magazine,
Vol. 00, No. 00, DD Month 200x, 1–25

High pressure torsion applied to nickel single crystals

Martin Hafok, Reinhard Pippan *

Jahnstraße 12, A–8700 Leoben, Austria

(v3.1 released April 2006)

Nickel single crystals with different crystallographic orientations were deformed by high pressure torsion. Special attention is devoted to examining the evolution of the micro-texture and microstructure. The initial crystal orientation was found to have a significant effect on the mechanical hardening and evolution of micro-texture at low and medium equivalent strains, whereas at very high strains no effect of the initial orientation was observed and the behaviour was very similar to a polycrystal. The evolution of micro-texture is in good qualitative agreement with the full constrained Taylor model. At very high equivalent strains the initial crystal orientation has no influence on micro-texture. At such strains the hardening, the refinement of the structure and the texture reaches a saturation. The final micro-texture is explained by the change from one preferred crystallographic orientation to another.

For Peer Review Only

1 Introduction

Several severe plastic deformation techniques allow the production of submicron or nanocrystalline bulk materials. The most popular techniques are equal channel angular pressing (ECAP) and high pressure torsion (HPT), where polycrystalline metals are typically used as starting materials [1, 2]. In the polycrystalline aggregate the individual crystallites are affected differently when they are subjected to plastic shear strain, i. e. a crystallite of the aggregate deforms against the resistance of the adjacent grains. A result of this inhomogeneous deformation is the pile-up of dislocations at grain boundaries, this induces stresses on the neighbouring grains and may activate further dislocation sources. Due to the increase in dislocation density within the grains the formation of strain-induced boundaries is promoted. As a consequence, the new dislocation arrangement within the grains disrupts the initial crystallographic orientation and contributes to grain fragmentation.

In the case of a single crystal, with a low dislocation density ($10^5 cm^{-2}$) [3], the dislocation glide is not constrained by boundaries in the early stages of deformation. Therefore, in the present work, the absence of initial boundaries and the effect of the overall initial orientations of the crystals should aid in the understanding of the micro-textural evolution during severe plastic deformation.

Single crystals have been used in the field of severe plastic deformation in a few studies on equal channel angular pressing to identify the activation of glide systems and the influence of friction in the vicinity of the die walls [4,5]. However, single crystal experiments with HPT have not been reported in the literature. In the HPT process the deformation of the sample is inhomogeneous, due to the existence of a strain gradient in the radial direction. This strain gradient is a major characteristic of the process due to the continuously increasing degree of deformation in the radial direction of a disc-shaped sample subjected to torsion around its cylinder axis. During deformation slipping of the disc is prevented by the application of a high compressive force which induces a high hydrostatic pressure within the sample. This hydrostatic pressure, which all severe plastic deformation techniques have in common, is the reason that very high plastic strains can be achieved without fracture of the material [6–8].

*Corresponding author. Email: pippan@oeaw.ac.at

Philosophical Magazine
ISSN 1478-6435 print/ISSN 1478-6443 online © 200x Taylor & Francis
http://www.tandf.co.uk/journals
DOI: 10.1080/1478643YYxxxxxxxx

2 Experimentals

Single crystal discs of nickel, with crystallographic orientations <0 0 1> and <1 1 1> parallel to the disc axis, were produced from high purity material with diameter $14mm$ and height $0.8mm$. The discs were placed in the cavity between two dies aligned in the vertical direction, these dies can be readily exchanged in order to process different sample sizes. Upon initial compressive loading the sample material fills the cavity and some excess material flows out between the two dies, this is due to the difference in cavity depth of the dies, $0.6mm$, and the original sample height, $0.8mm$. After compression the upper die remains in a fixed position while the lower die rotates around its cylinder axis in order to apply a shear strain to the sample. During the HPT-deformation the gap between the two stamps is not fully closed. In particular, at the commencement of the shear deformation additional excess material can flow out until the lower and upper stamp are in contact with each other. At this point the sample height remains constant between 0.6mm and 0.7mm and no additional sample material is lost during the deformation. The influence of the shear on the reduction of sample thickness under high pressure was examined in [9]. In this paper the Bridgman rotating-anvil shear press was used to observe the influence of the applied pressure on the shear stress and on the reduction of the sample thickness. The Bridgman rotating-anvil shear press is very similar to the HPT device, but the shear press is unable to exert a high hydrostatic pressure during the sample deformation. This missing feature makes a direct comparison of the material behaviour measured by these two methods questionable, despite hydrostatic pressure being only a weak influence on material behaviour during HPT-deformation. However, the applied pressure influences the friction between the dies and the excess material and therefore contributions to the measured torque. For a more detailed description of the high pressure torsion process can be found in [10, 11].

Due to the torsion exerted on the small metallic discs the initial orientation of the single crystal is rotated around the torsion axis as a function of the disc height and the twist angle θ. In figure 1a such a rotation is indicated at the left side of the drawing. The cubes represents the initial orientation of the single crystal which are constantly rotated around the torsion axis due to the torsion deformation. However, the initial orientation is constant within a layer whose plane normal lies parallel to the torsion axis.

A simple mathematical description can be used to describe the torsion deformation of a cylinder, this is equally applicable to the discs used in the HPT-deformation experiments presented here [12]. Careful alignment of the dies ensures rotation around the disc axis and hence the disc cross-section is invariant with applied strain. The bottom of the disc is displaced by an angle of twist θ with respect to the top by shearing of the structural elements by an angle γ, as shown in figure 1a. For shear strain measurement the shear angle γ is referred to as an equivalent strain ϵ_{eq}, calculated as follows:

$$\epsilon_{eq} = \frac{\gamma}{\sqrt{3}} \tag{1}$$

In this study the single nickel discs were deformed by HPT at room temperature. The angular velocity of $0.025min^{-1}$ and pressure of approximately $2.3GPa$ were kept constant for all samples. In order to provide a detailed examination of how the micro-texture and microstructure evolves nickel single crystals were deformed to two different equivalent strains. The samples were deformed to an equivalent strain corresponding to the commencement of saturation on the torque curves, as can be seen in figure 2, and to full saturation, such that the saturated microstructure extends over nearly the whole sample. Nickel single crystals with an initial crystallographic orientation of <1 1 1> and <0 0 1> parallel to the disc axis were chosen for HPT and deformed to equivalent strains of 32 at a radius of $6mm$, as listed in table 1.

The evolution of microstructure and micro-texture was extensively studied by electron backscatter diffraction (EBSD) measurements. These measurements were performed with a field emission gun scanning electron microscope ZEISS® 1525 equipped with an EDAX® EBSD system. In order to obtain qualitatively good diffraction patterns all sample surfaces were electrolytically polished using a A2 (Struers®) electrolyte.

The quality of an EBSD scan is dependent on the magnification and, more importantly, on the plastic distortion of the scanned region. In our measurements we achieved an indexing fraction of nearly 100% for

For Peer Review Only

the less deformed regions (ϵ_{eq} between 0.5 to 3) while for the more heavily deformed regions (ϵ_{eq} between 10 to 32) we obtained a indexing fraction between 85% and 90%.

The EBSD measurements can be divided into (i) measurements in the radial direction, (ii) measurements in the tangential direction and (iii) measurements that were carried out on a cut plane. In figure 1b the position of the measurements in the radial direction and the tangential direction are shown. These measurements were recorded in top view while the measurements performed on the cut plane were obtained in side view, as shown in figure 1a. The EBSD measurement position used in top view were defined by the angle φ and the radius r.

In the schematic illustration of the disc, figure 1b, the rectangles symbolize the areas measured by an EBSD scan. For EBSD scans taken in the radial direction the strain experienced by the samples at each point is different. Measurements in the tangential direction are of material strained to the same degree but with different initial crystallographic alignment parallel to the shear direction. The alignment of the scanned regions corresponds to the rotation angle φ at a constant radial distance. The final type of measurement was carried out near the centre of a cut plane in the sample, indicated by a dotted line in figures 1a and 1b this cut plane was made at a varius radii.

3 Results

3.1 *Mechanical response*

During HPT deformation the torque on the single crystalline disc was measured using a load cell, that was specially designed for the HPT apparatus. The load cell allows measurement of torque applied to the material without significant contribution from the testing machine, other than the friction due to excess material flowing out from the cavity after the initial compressive loading. Consequently, an estimation of the shear stress and the hardening behaviour is possible. A detailed analysis of the yield stress determination is described in [6].

In figure 2 the torque vs. equivalent strain curves are plotted. The curves differ with respect to each other due to the different initial crystallographic orientations of the single crystals and the crystallographic orientation distribution in the polycrystalline nickel. The difference in torque due to the different initial crystallographic orientations can be explained by considering Schmids law [13, 14].

$$m_{ij}^{(s)} = \frac{1}{2}\left(b_i^{(s)} n_j^{(s)} + b_j^{(s)} n_i^{(s)}\right) \tag{2}$$

$$m_{ij}^{(s)} \sigma_{ij} = \tau_{CRSS}^{(s)} \tag{3}$$

In equation 2 the variable **b** denotes the glide direction and **n** is the glide plane normal. The equation 3 demands that slip of a dislocation under an applied stress tensor $\boldsymbol{\sigma}$ is only possible if the critical resolved shear stress (CRSS) of the glide system is reached. In the last equation the Einstein summation convention was used.

A torsion deformation is characterised by a symmetric Cauchy stress tensor $\boldsymbol{\sigma}$ that includes only two non-diagonal elements τ symbolising the applied shear stress. When equation 3 is divided by the applied shear stress, τ, and evaluated for single crystals with <1 1 1> and <0 0 1> directions parallel to the torsion axis, considering all orientations that can be obtained by rotating around the torsion axis, the maximum values of this Schmid factor are1.0 and 0.577 respectively. In order to reach the critical resolved shear stress the applied shear stress of the <0 0 1> oriented single crystal must be nearly twice the magnitude of the applied shear stress of the <1 1 1> oriented single crystal. These results agree with the measured torque curves in figure 2.

In figure 2, the torque curves of the single crystals reach the same value in saturation while the nickel polycrystal reaches a saturation torque approximately $20Nm$ higher. This difference can be accounted for

For Peer Review Only

by the larger grain size of the higher purity single crystals in the saturation region compared to that of the lower purity nickel polycrystal.

3.2 *Micro-texture and Microstructure development*

Using an EBSD system the distribution of crystallographic orientation with plastically deformed regions can be readily measured. The EBSD-data qualitatively assess the deviation from the original orientation and permits a quantification of the development of strain induced boundaries. However, these cannot be directly interpreted as a measure of plastic strain because one does not gain information about the strain from the misorientation gradient or the change of the initial orientation.

The micro-textures and microstructures of the nickel single crystals were recorded in the radial direction, the tangential direction and near the middle of the cut plane as described earlier. The alignment of the EBSD scans is indicated by a coordinate system, where "TAN" represents the tangential direction, "RAD" the radial direction and "TOR" the torsion axis that is parallel to the cylindrical axis of the disc and perpendicular to the plane containing the radial and tangential direction. The initial crystallographic orientations of all single crystals are given with respect to this coordinate system.

The EBSD orientation data can be concerted to boundary maps and micro-textures. Figure 3 shows a grain boundary map, with the associated (0 0 1) pole figure, of the nickel <1 1 1> single crystal recorded parallel to the HPT torsion axis. The scan data obtained from this $30\mu m$ x $30\mu m$ area corresponds to an equivalent strain of 1.5. The small scan size ensures that the difference in global shear strain between the left side and the right side of the boundary plot is negligible, the difference of equivalent strain due to the difference in radius between the left and the right side of the inverse pole figure map corresponds to a value of only 3%.

The microstructural evolution in the boundary plot in figure 3a shows a region of locally enhanced accumulated lattice rotation (RLALR) in the centre. A darker boundary in the plot corresponds to a greater angular misorientation between neighbouring structural elements. In order to differentiate between the RLALR, bordered by dark lines representing high angle boundaries, and the regions with less orientation change the boundary plot is marked with the letters A, B and C. In this plot B corresponds to the RLALR, indicated by a higher density of low angle boundaries arranged in an elongated cell shaped structure.

Figure 3b shows the (0 0 1) pole figure. Pole figures are usually defined with respect to the normal direction and the rolling direction. In the case of torsion under hydrostatic pressure such a definition can lead to confusion, accordingly another convention to represent crystallographic orientations is used. Here the texture indices are defined with respect to the torsion axis and the tangential direction. Using this convention the round brackets symbolise the crystallographic plane parallel to the torsion axis and square brackets indicate the crystallographic direction parallel to the tangential direction. This convention is used in all the tangential and radial measurements presented here.

In the (0 0 1) pole figure the initial orientation indicated with white squares is of the kind (1 1 1) [3 -2 -1] with respect to the defined coordinate system. The spread of crystallographic orientation, about 12°, around the initial crystallographic orientation is associated with plastic deformation of the regions A and C in figure 3a. The change of the crystal orientation of these regions is relatively low in comparison to region B, where the crystallographic orientation is rotated from the initial crystallographic orientation to the (-1 -1 -1) [-3 1 2] orientation, marked with white circles. This rotation is indicated by a trace like orientation distribution connecting the initial crystallographic orientation and the crystallographic orientation of the regions with locally accumulated lattice rotations.

3.3 *Micro-texture evolution in the tangential direction*

Performing EBSD-scans at the same radius around the sample, i.e. in the tangential direction, allows for orientation plots at different areas on the sample with the same magnitude of plastic shear strain. However, the relation between the shear direction, parallel to the tangential direction, and the initial crystallographic orientation, which changes between individual measurement positions, determine the evolution of micro-texture.

For Peer Review Only

In figure 4 pole figures of the nickel <1 1 1> single crystal recorded in the tangential direction show the micro-texture development. The pole figures were obtained from 200μm x 200μm large EBSD scans that correspond to an equivalent strain in the range of 1.4 to 1.6. The tangential measurements were started at an arbitrary angle denoted the $\varphi = 0°$ position. After each scan the sample was rotated by an angle of $\varphi = 30°$ up to a maximum angle of $\varphi = 120°$. Because of the rigid sample rotation between the different scans the initial crystallographic orientation in the pole figures is also rotated by the same amount after each scan. In order to illustrate the sample rotation two poles of the initial crystallographic orientation are labelled A and B.

In figure 4a, at the $\varphi = 0°$ position, the initial crystallographic orientation of the nickel <1 1 1> single crystal is indicated by white squares. The RLALRs have changed the crystallographic orientation to a position marked by the white circles. This orientation is close to the centre of the (0 0 1) pole figure. These two orientations are connected by a streak-like orientation distribution similar to the micro-texture in figure 3b. At a rotation angle of $\varphi = 30°$ around the torsion axis, figure 4b, the orientation of the RLALR deviates from the centre of the (0 0 1) pole figure and therefore occupies a completely different crystallographic orientation with respect to the 0° position. Further pole figures, evaluated from EBSD-scans at different φ-rotations of the <1 1 1> nickel single crystal, are shown in figures 4c-e. Here the orientations of the RLALRs approach once more the centre of the (0 0 1) pole figure in the 60°, 90° and also the 120° position.

The micro-texture in the $\varphi = 120°$ position is very similar to the micro-texture recorded at a rotation angle of $\varphi = 0°$. Due to the similarity in micro-texture development of the $\varphi = 0°$ and $\varphi = 120°$ positions additional pole figures were recorded up to an angle of $\varphi = 240°$ and analysed in the same manner. From these observations it can be concluded that the micro-texture develops a threefold symmetry at this specific equivalent strain. Furthermore the <0 0 1> orientation is approached in the majority of the EBSD scans, indicating a preferred orientation.

The same measurement procedure was applied to the <0 0 1> nickel single crystal. In figure 5 the micro-texture development in the tangential direction is shown. The first 200μm x 200μm scan was carried out at an arbitrary point corresponding to an equivalent strain between 1.4 and 1.6. All following 200μm x 200μm large scans were recorded on the same radius but at different positions corresponding to different sample rotations φ. In the (0 0 1) pole figures the initial orientation and the orientation of the RLALRs are indicated by white squares and white circles respectively.

The first pole figure shown in figure 5a represents a micro-texture developed at a sample rotation of $\varphi = 0°$. In the pole figure the initial orientation is represented by the (0 0 1) orientation and the orientation of the RLALRs correspond to a (1 1 1) orientation, which can be obtained by rotating the initial crystallographic orientation around the radial axis. If we consider figure 5b, evaluated after rotating the sample by an angle of $\varphi = 30°$ around the torsion axis, we can see that the initial orientation, also rotated by 30°, deviates from the centre of the pole figure plot by an angle of approximately 15°. This deviation may be caused by the small misalignment of 3° between the initial <0 0 1> orientation and the torsion axis combined with the low stability of the preferred orientations. In this pole figure the orientation of the RLALRs were found to occupy an orientation close to the (0 1 1) orientation, this is also found in the $\varphi = 60°$ position. In figure 5d the sample is rotated by $\varphi = 90°$ and the pole figure depicts a similar micro-texture as in the 0° position (figure 5a), this clarifies the repetition of the micro-texture development and the evolution of a fourfold symmetry at this particular equivalent strain. In addition to the evolution of a characteristic micro-texture one pole of the RLALRs can be considered as a common rotation axis for all these regions. This pole, marked by the letter A in the pole figures, deviates by an maximum angle of 20° between the individual EBSD scans.

For further analysis of preferred orientation the fraction of data attributed to the initial alignment and the region of larger orientation change with respect to the sample rotation, φ,is considered in figure 6. In these plots the orientation density is given in units times random. In figure 6a the orientation density of the nickel <1 1 1> single crystal is shown up to a rotation angle of 120°, the squares representing the orientation density of the initial orientation and the circles corresponding to the orientation density of the RLALRs. This plot depicts a shift of the orientation density from the initial orientation (between 15° and 60°) to the RLALRs (ranging from 75° to 120°). In contrast to the micro-texture evolution of the nickel

For Peer Review Only

<1 1 1> single crystal, the <0 0 1> single crystal shows no shift to another alignment, but instead a variation in orientation density of the initial orientation. The <0 0 1> orientation density deceases from $\varphi = 0°$ up to an angle of 45°, this is followed by an increase nearly symmetric increase up to $\varphi = 90°$. The orientation density of the RLALRs is not significantly influenced by φ, figure 6b.

3.4 *Comparison with the Taylor model*

A simple model to predict the development of crystallographic orientations was given by Taylor [15]. His model is based on the assumption that all crystallites are subjected to the same plastic strain, achieved by multiple slip. By using the Taylor model the texture evolution is calculated incrementally [14] and the results were indicated by open circles in a calculated (0 0 1) pole figure plot. In the case of a fcc material only glide systems of the kind {1 1 1} <0 1 1> are considered. The deformation correlated with the HPT deformation is given by the distortion tensor $\boldsymbol{\beta}$ [17]:

$$\boldsymbol{\beta} = \begin{pmatrix} -e/2 & 0 & 0 \\ 0 & -e/2 & \gamma \\ 0 & 0 & e \end{pmatrix} \tag{4}$$

Here γ is the shear deformation and e represents the flow of the excess material at low equivalent strains during HPT. The calculation is based on a single initial orientation rotated around the torsion axis simulating the distortion of the crystal system with respect to the φ-position in the experiment.

The result of such a calculated texture is shown in figure 7b, figure 7a depicts a measured micro-texture of the <1 1 1> nickel single crystal at an equivalent strain of 2.5 and e = 15% for comparison. The experimental and the calculated pole figures both had an initial crystallographic orientation of (1 1 1) [1 1 -2]. Examination of the orientation spread beginning at the initial crystallographic orientation shows that the density of calculated and measured poles is distributed inhomogeneously. The initial orientation, marked by white squares, has nearly vanished in the measured pole figure as most structure elements rotated into the (0 0 1) [-1 1 0] orientation. In the radial measurements of the <1 1 1> nickel single crystal the same orientation was preferred, indicated by white circles in the (0 0 1) pole figure. A further increase of shear strain promotes the reorientation of the structure elements into the second preferred orientation (1 1 1) [-1 2 -1], indicated by white stars.

A similar texture is obtained by a calculation based on the Taylor model. In the computation the poles are arranged in trace-like orientation distribution. Furthermore, the maximum density of calculated poles occupies close to the same orientations as shown in the measured pole figure. In addition to the orientation distribution of the calculated (0 0 1) pole figure the equivalent strains that correspond to the different orientations are also given, figure 7b. By using the calculated results it can be seen that the (0 0 1) [-1 1 0] orientation is maintained over a wide range of equivalent strains ranging from 0.6 to 2.2, indicating a stable orientation. Furthermore, the (1 1 1) [-1 2 -1] orientation, the second preferred orientation, appears in the measured pole figure at an equivalent strain of about 3 to 3.5. This value exceeds the average equivalent strain of 2.5. An explanation can be given by considering the inhomogeneous deformation, with some regions experiencing a higher or lower shear strain but the average of these local variations in shear strain must be in accordance with the global equivalent strain imposed at the particular radius.

Owing to the good correlation of the Taylor model with the measurements in figure 7, calculations were performed to determine the micro-texture development of the <1 1 1> and the <0 0 1> orientations in the tangential direction (figures 8 and 9). The initial crystallographic orientation used for the calculations was rotated in 30° intervals about the torsion axis, this significantly affected the micro-texture evolution.

All calculations were performed incrementally up to an equivalent strain of 1.5, which corresponds to the maximum equivalent strain in the tangential measurements. The calculated and measured texture evolution of the <1 1 1> nickel single crystal in the tangential direction show strong similarity, as can be seen by a comparison of figures 4 and 8. The density distribution of the poles that evolved in the calculation is also confirmed by the measurements. However, the computed results do deviate from the

For Peer Review Only

measured micro-textures in some ways. The deviations in micro-texture between figures 4 and 8 are a consequence of the development of the preferred orientation, which is achieved earlier in the experiment. A comparison between the calculated and measured micro-textures of the <0 0 1> nickel single crystal, shown in figures 5 and 9 respectively, also reveals deviations. The differences in these figures are due to experimental scatter of the measured poles in the radial direction, figures 8b and 8c. The simple Taylor model is unable to predict such scatter because the interaction between individual structure elements is not considered. On the other hand, the $\varphi = 0°$ and $\varphi = 90°$ positions in figures 9a and 9d demonstrate good accordance between calculation and measurements.

3.5 *Micro-texture evolution in the radial direction*

The strain gradient in the radial direction allows measurements for different degrees of deformation by examining only one sample. Measurements were recorded at various radii, corresponding to different equivalent strains, without sample rotation. The results of the radial micro-texture scans are shown in figure 10. In the pole figures the initial crystallographic orientation of the <1 1 1> nickel crystal is (1 1 1) [1 1 -2].

The HPT deformation leads to a micro-texture with a particular orientation distribution, appearing as streaks in the pole figure. The streaks connect the initial crystallographic orientation, white squares in the pole figure, and the RLALRs, white circles. The micro-texture evolution in the radial direction shows that certain crystallographic orientations are approached. The first preferred orientation is shown in figure 10b. If an equivalent strain of 2 is exceeded the streaks extend to the next, or second, preferred orientation (white stars in figure 10c). With increasing equivalent strain more regions occupy an orientation close to the second preferred orientation, as can be seen through a comparison of figures 10c and 10d.

Before the equivalent strain reaches the saturation region of the torque curves the second preferred orientation (white stars in figures 10c and 10d) becomes smeared out. If the equivalent strain exceeds the onset of the saturation region the first preferred orientation also becomes more diffuse. Nevertheless, a maximum in the centre of the (0 0 1) pole figure is still visible, as can be seen in the figures 10f to 10h. In order to provide a better understanding of the micro-texture development in the saturation region it is necessary to consider a measurement recorded near the centre of a cut plane, similar to the cut plane in figure 1. Such a (1 1 1) pole figure with an equivalent strain of 32 is shown in figure 10i. Furthermore, it has to be noted that this scan was recorded in side view and is therefore aligned in the tangential direction and in the direction of the torsion axis. The crystallographic orientation distribution of figure 10i represents a shear texture and was recorded at the same equivalent strain as the pole figure in figure 10h. These two pole figures do not appear similar on the first view, but this difference is due to the different kind of crystallographic planes used to depict the micro-textures. But it is emphasized that these two pole figures represent the same distribution of crystallographic orientations with respect to the sample coordinate system. From these observations, it can be concluded that the development of a shear texture starts at the beginning of the saturation region of the torque curve.

3.6 *Microstructure development in the radial direction*

In the previous sections the evolution of the micro-texture was examined, but in order to reveal additional aspects of the fragmentation process it is necessary to consider the evolution of the microstructure. Therefore, orientation maps in the radial direction of the <1 1 1> nickel single crystal were analysed to examine the microstructure evolution with increasing equivalent strain. The results of the $30\mu m$ x $30\mu m$ EBSD-scans performed in top view were evaluated as boundary and inverse pole figure plots as shown in figure 11. In the plots the darkness of the boundaries correspond to different misorientation angles, darker being a greater misorientation, between neighbouring structure elements and the colours correspond to different orientations in the inverse polefigure as shown below.

In the case of a single crystal no boundaries are present in the as-received state. All boundaries, formed during deformation, are induced by plastic strain. Due to the increase in dislocation density during deformation a few low angle boundaries were formed. These boundaries consist of a band shaped structure

For Peer Review Only

aligned in the radial direction. The bands get more pronounced with increasing strain, as can be seen in figure 11b. In the centre of this boundary plot a band has evolved that is bordered by high angle boundaries, while the interior of the band is subdivided by a cell structure consisting of low angle boundaries. Outside the band the initial crystallographic orientation is distorted weakly, indicated by the low density of low angle boundaries. With increasing equivalent strain the bands subdivide, due to the formation of high angle boundaries, and the structure in between transforms to an equiaxed cell structure of low angle boundaries at an equivalent strain of about 3. After a further increase of the equivalent strain the microstructure starts to shift from bands to a structure of elongated grains bounded by high angle boundaries and subdivided into a cell structure consisting of low angle boundaries. This microstructure decreases its size until the saturation region of the torque curve is reached. At an equivalent strain of 12 most of the structure elements have developed a minimum structure size, which is in the order of magnitude of the cell size. This minimum structure size cannot be further decreased by deformation, as is apparent through a comparison of figures 11g and 11h. These show two microstructures recorded at equivalent strains corresponding to the saturation region of the torque curve.

In order to examine the formation of bands at low equivalent strains, and to compare the microstructure with the saturated microstructure, the side view of the sample through a cut plane was chosen, as shown in figure 1a. The microstructure in figure 12a, which corresponds to a relative low equivalent strain of about 2.5, shows highly elongated structure elements. These correspond to the bands in the radial measurements performed on the top side of the disc. These bands were all tilted by an angle of approximately 75° with respect to the torsion axis, which is in good agreement with the imposed shear deformation of $\epsilon_{eq} = 2.5$. As reported, the bands are subdivided by an elongated cell structure, formed by low angle boundaries, and aligned in the tangential direction with a deviation of approximately 15°. The comparison with the saturation microstructure in figure 12b indicates that the misalignment of the cell structure with respect to the shear or tangential directions seems to be unaffected by the fragmentation process. The figure shows structure elements with an average length of 340nm and an average height of 170nm. If the same microstructure is shown in a different view, as in figure 11i, the structure elements appear more or less equiaxed. Hence the structure elements have an ellipsoidal shape, wherein the two minor axes are of approximately equal length and the major axis is tilted with respect to the torsion axis by an angle of approximately 75°.

The dependence of structure size on the radial distance, and hence equivalent strain, of the <1 1 1> nickel single crystal is shown in figure 13a. Here boundaries higher than 15° are considered as borders of structure elements and the measurements are from the top surface of the disc. As the the two nickel single crystals reduce their structure size in a similar manner are combined in the evaluation. The curve depicts a decrease in structure size until an equivalent strain corresponding to the onset of the saturation region of the torque curves in reached. The structure size in this region of saturation is around 380nm.

The development of boundary length, of different misorientation angle, per unit area as a function of the equivalent strain is shown in figure 13b. The data was evaluated from EBSD scans of the nickel <1 1 1> single crystal already used to show the microstructure development in figure 11. In figure 13b boundaries with misorientation angles higher or lower than 15° are referred to as high angle or low angle boundaries respectively. The graph shows a sharp increase of the low angle boundary density at low equivalent strains. At an equivalent strain of 3 a maximum is reached, where 70% of all boundaries have a misorientation angle lower than 15°. The density, and also the fraction, of high angle boundaries increases with an increase of the equivalent strain up to the saturation region of the torque curve. In this regime the fraction of high angle boundaries has reached an almost constant value of about 85%.

The fragmentation of the original microstructure and the increase in boundary density, due to the HPT-deformation, leads to an increase of the misorientation angle between adjacent structure elements. In figure 14a the misorientation distributions for different equivalent strains are shown. In addition, the misorientation of a random orientation distribution (McKenzie curve) is indicated by a thick black line. At the very low equivalent strain of $\epsilon_{eq} = 0.5$ no high angle boundaries exist and the distribution shows a strong decline up to a misorientation of approximately 10°. By increasing the equivalent strain the density of low angle boundaries and also the misoriention angle between different structure elements increases. This leads to a second peak is at a misorientation angle of approximately 53°, indicating the formation of high

For Peer Review Only

angle boundaries during deformation. The mean values of the misorientation distributions corresponding to different equivalent strains are shown in figure 14b. In the graph the dashed line refers to the average of the MacKenzie curve. It is obvious that the average misorientation value in the saturation regime in figure 14b deviates by about 3° from the average misorientation of the MacKenzie curve.

4 Discussion

The micro-texture and microstructure evolution of nickel single crystals was studied by the application of the EBSD technique. It is well known that the evolution of microstructure and micro-texture is governed by the initial structure of the material, its mechanical properties, the deformation temperature, the mode of plastic deformation and the strain rate [18]. In this study all samples were deformed at room temperature and all specimens were subjected to the same rotational speed, accordingly the influence of strain rate on the micro-texture and microstructure evolution was not examined explicitly.

The EBSD scans reveal regions of locally enhanced accumulated lattice rotation appearing as bands at relatively low equivalent strains. The locally enhanced accumulated lattice rotation of these regions can originate due to small deviations in the microstructure away from the initial crystallographic orientation. These variations are caused by the formation of dense dislocation walls, cell walls and microbands which is a well known phenomena in other single crystal deformation experiments [19]. Such variations in the initial orientation can be introduced during or after the manufacturing process and manifest as low dislocation densities or as small misorientation gradients. However, these crystallographic deviations are negligible in comparison to the changes that occur at the commencement of HPT deformation where the strong crystallographic orientation distribution is smeared out around the initial points. This smearing out of crystallographic orientations causes small changes in the micro-texture that result in small variations of the Taylor factor. Accordingly, regions with different Taylor factors have different mechanical behaviors and so deformation becomes localised to softer areas. For example, consider the evolution of the Taylor factor based on the EBSD scan data that is shown in figure 3. A Taylor factor of about 3.2 was obtained for the weakly distorted regions, A and C, while region B received a Taylor factor between 2.5 and 3. Therefore this band deforms more easily than the harder, regions A and C.

In the micro-texture evaluation this locally enhanced accumulated lattice rotation in figure 3 is indicated by the continued existence of the initial orientation even after the sample was subjected to a large shear strain. In addition to this a trace can be seen in the pole figure joining the initial orientation to the preferred orientation. A comparison between the pole figure and the recorded microstructure indicates that the trace-like distribution of crystallographic orientations is due to a band-shape structure, while the crystallographic orientation of the surrounding matrix is spread weakly around the initial orientation.

Such a micro-texture evolution can also be computed by the use of the full constrained Taylor model, implying that all structure elements are deformed by the same macroscopic shear strain. In the Taylor model a Taylor hardening of the glide systems is assumed, which does not account for the interaction between the different glide systems. The comparison between calculated texture evolution and the measured micro-texture development fits well. This is despite the interaction of structural elements not being modeled, which may cause the deviations between the measurement and the calculation. Nevertheless, the results are in good agreement with the measurement so we can conclude that the interaction of structural elements becomes more important at higher equivalent strains as shown in figures 10g-i. In these figures a shear texture has evolved due to the fragmentation and interaction of structural elements that are bordered by high angle boundaries. In addition, the misorientation distributions evaluated at different equivalent strains deviate from the random distribution (MacKenzie curve) in figure 14a. At low equivalent strains this is due to the strong influence of the initial orientation while at high strains it can be attributed to the formation of a shear texture.

In this regime the shear texture, which is typical for high pressure torsion and equal channel angular pressing samples at very high strains [20], may be explained in the following way. The different crystallites change their orientation to a preferred orientation. The crystallites can maintain the preferred crystallographic orientation during shear. However, such a preferred orientation is not stable, hence the crystal orientations changes to another preferred orientation. This phenomenon is clearly visible in the evolution

For Peer Review Only

of micro-texture in the differently oriented single crystals and also from the full constrained Taylor model as discussed above. Such a mechanism promotes fragmentation of the microstructure [21].

Finally, it was shown that the fragmentation process is not a result of the different distortion of different crystallites. The fragmentation is caused by the formation of a cell structure independently of the existence of grain boundaries. The grain boundaries facilitate the fragmentation [22], but they do not influence the onset of the saturated microstructure or the saturated grain size. Nevertheless, the details of the formation of the saturation microstructure have not been clear until now. A possible explanation would be a combination of dislocation movement and a stress driven boundary migration process. The first mechanism drives the fragmentation and the structure refinement while the second mechanism promotes recovery and the growth of structure elements. In the saturation regime of the torque curves both mechanisms have reached an equilibrium state, leading to constant structure size.

5 Summary

- The initial orientation has a significant effect on the evolution of the strength, the micro-texture and microstructure only for equivalent strains less than 10.
- The evolution of the micro-texture follows the prediction of a full constrained Taylor model in this deformation regime. Band-like structures develop during deformation, nethertheless, the orientation in these bands also follows the Taylor prediction.
- The structural elements rotate into preferred orientations. However a crystallographic orientation located at a preferred orientation is not stable, therefore the crystallographic orientation changes from one preferred orientation to another preferred orientation.
- The developed "deformation" bands subdivide and become more narrow with increasing equivalent strain, until the structure size does not decrease any further. At this stage the band like structure transforms to a more equiaxed structure.
- The saturation of the microstructure coincides with the saturation of the hardening.
- The initial crystallographic orientation does not affect the onset of saturation.

6 Acknowledgement

The financial support by the Austrian Fonds zur Förderung der wissenschaftlichen Forschung (Project: 17096 - N02) is gratefully acknowledged.

References

[1] Z. Yang, U. Welzel, Mater. Lett. **59** 3406 (2005).
[2] M. J. Zehetbauer, J. Kohout, E. Schafler, F. Sachslehner, A. Dubravina, Journal Alloys Compd. **378** 329 (2004).
[3] Y. Miura, F. Higuchi, H. Era. Philos. Mag. A. **71** 1363 (1995).
[4] H. Miyamoto, J. Fusimi, T. Mimaki, A. Vinogradov, S. Hashimoto, Mater. Sci. Eng. A **405** 221 (2005).
[5] M. Furukawa, Y. Kawasaki, Y. Miyahara, Z. Horita, T. G. Langdon, Mater. Sci. Eng. A. **410–411** 194 (2005).
[6] F. Wetscher, A. Vorhauer, R. Pippan, Mater. Sci. Eng. A. **410–411** 213 (2005).
[7] A. Vorhauer, R. Pippan, Scripta Mater. **51** 921 (2004).
[8] H. S. Kim, J. Mater. Process. Technol. **113** 617 (2001).
[9] B. C. Cai, D. Kuhlmann Wilsdorf, R.B. Nelson, Mater. Sci. Eng. A **138** 33 (1991).
[10] R. Z. Valiev, R. K. Isamgaliev, I. V. Alexandrov, Prog. Mater. Sci. **45** 103 (2000).
[11] A. Vorhauer, R. Pippan, Metall. Mater. Trans. A **39** 417 (2008).
[12] Timoshenko SP. Theory of Elasticity. (3rd Edition, Mc Graw-Hill, 1970).
[13] Schmid E, Boas W. Kristallplastizität. (Springer Verlag, Berlin, 1935).
[14] U. F. Kocks, Metall. Trans. **1** 1121 (1970).
[15] G. I. Taylor, J. Inst. Met. **62** 307 (1938).
[16] P. V. Houtte, E. Aernoudt, Z. MetaIlkd. **66** 202 (1975).
[17] J. Baczynski, J. J. Jonas, Acta Mater. **44** 4273(1996).
[18] U.F. Kocks, H. Mecking, Prog. Mater Sci. **48** 171 (2003).
[19] B. Bay, N. Hansen, D. A. Hughes, D. Kuhlmann-Wilsdorf, Acta Metall. Mater. **40** 205 (1992).
[20] S. Li, I. J. Beyerlein, D. J. Alexander, Mater. Sci. Eng. A **431** 339 (2006).
[21] H. P. Stüwe, Mater. Sci. Forum. **503–504** 175 (2006).
[22] M. Hafok, R. Pippan, Mater. Sci. Forum. **550** 277 (2007).

For Peer Review Only

Tables and figures

Table 1. Summary of the orientations and strains applied to nickel single crystalline samples.

Crystallographic orientation parallel to torsion axis	Disc diameter	Equivalent strain at radius 6mm	Number of turns
<1 1 1>	14mm	6	0.23
<1 1 1>	14mm	32	1.2
<0 0 1>	14mm	6	0.23
<0 0 1>	14mm	32	1.2

For Peer Review Only

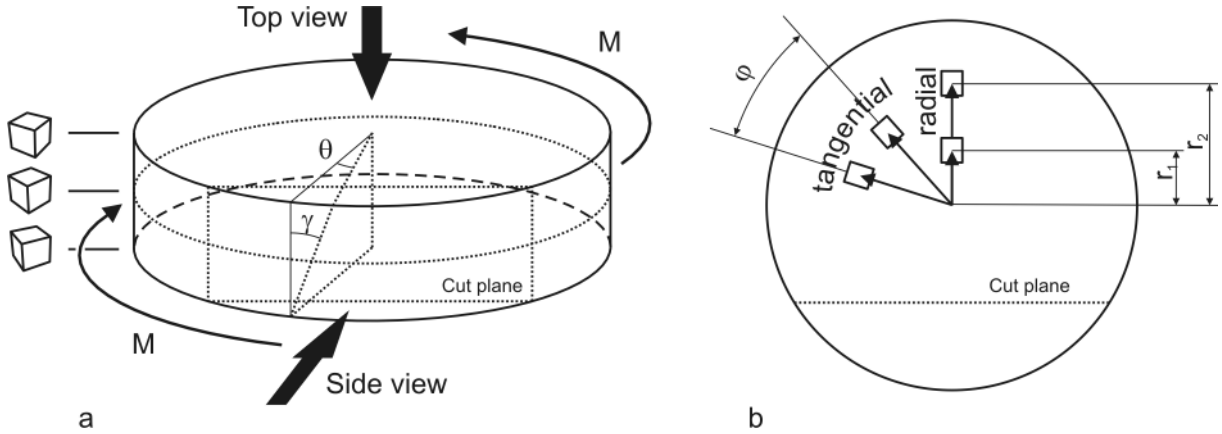

Figure 1. Schematic view of a single crystalline disc that is subjected to a torque M which shears the structure about a shear angle γ and a twist angle θ (a). The measurement procedure is divided in radial measurements and tangential measurements (b).

For Peer Review Only

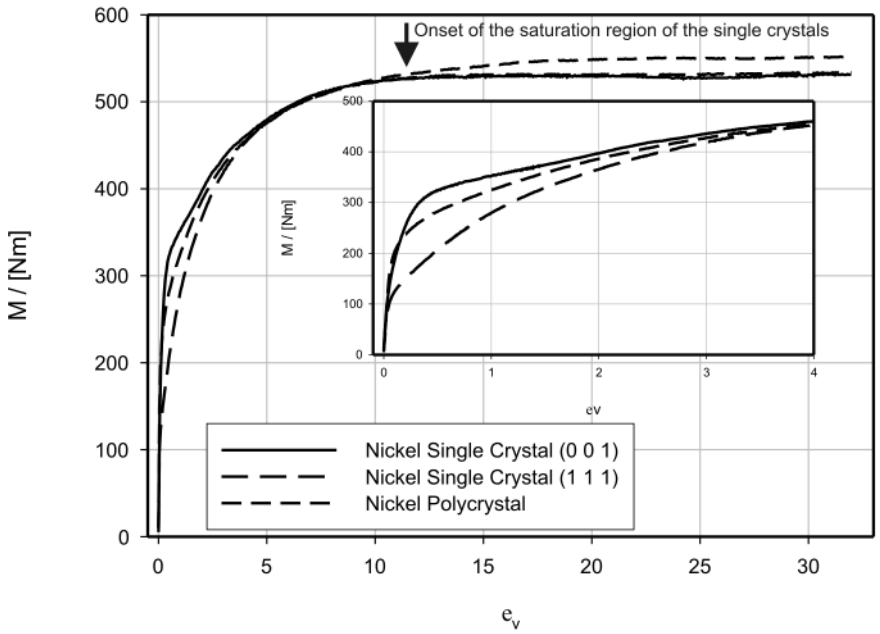

Figure 2. Torque vs. equivalent strain curves for nickel single crystals and nickel polycrystal. The equivalent strain corresponds to a radius of 6mm. The arrow in the plot indicates the onset of the saturation region.

Peer Review Only

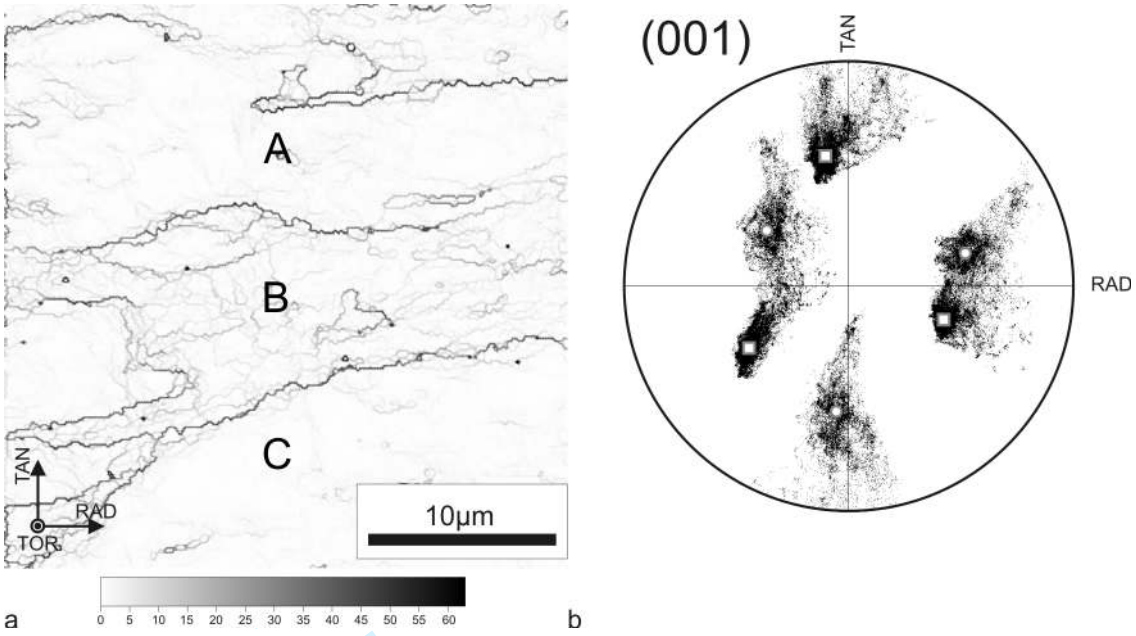

Figure 3. A boundary plot (a), where the darkness of the lines correspond to different misorientations of structure elements, and the associated (0 0 1) pole figure (b) is shown. For a description of the marked regions; A, B, C, please see the text. The 30μm x 30μmm scan was performed at an equivalent strain of 1.5.

Peer Review Only

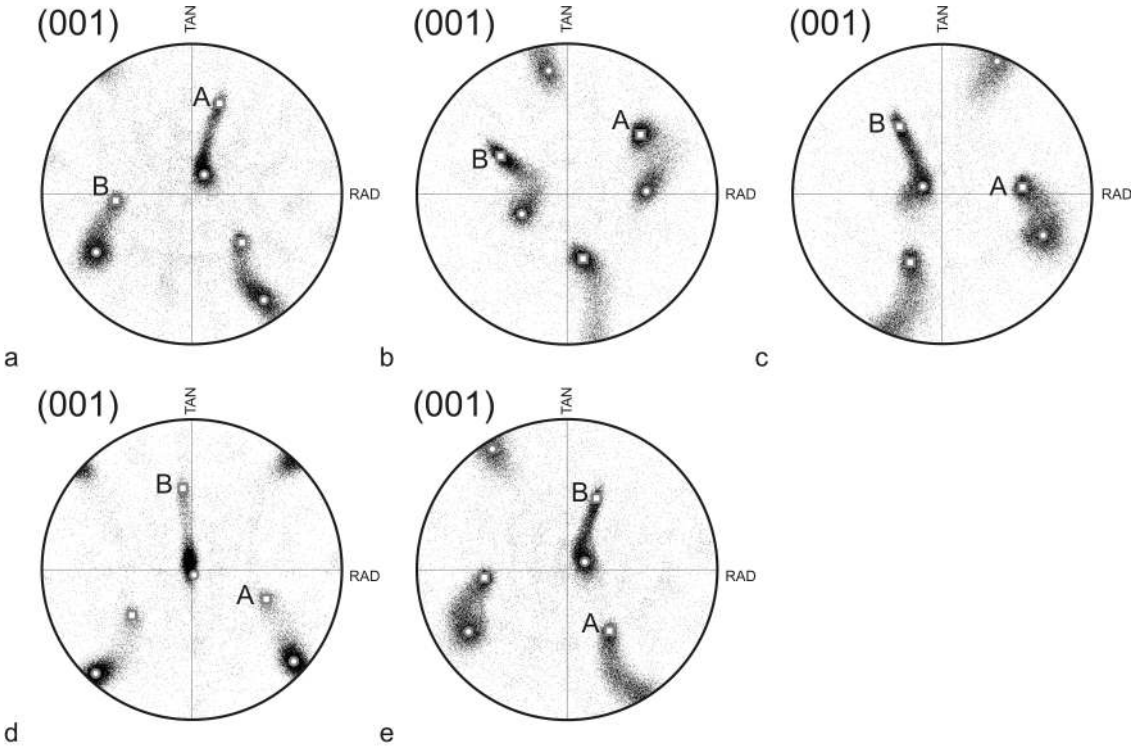

Figure 4. Texture development of the <1 1 1> nickel single crystal in the tangential direction at an equivalent strain of 1.5. The (0 0 1) pole figures were evaluated from EBSD measurements of a 200μm x 200μm area and correspond to a sample rotation of φ = (a) 0°, (b) 30°, (c) 60°, (d) 90°, (e) 120°. The white squares mark the initial orientation while the white circles indicate the crystallographic orientation present in regions of enhanced accumulated lattice rotation. The letters A and B mark poles of the initial orientation

For Review Only

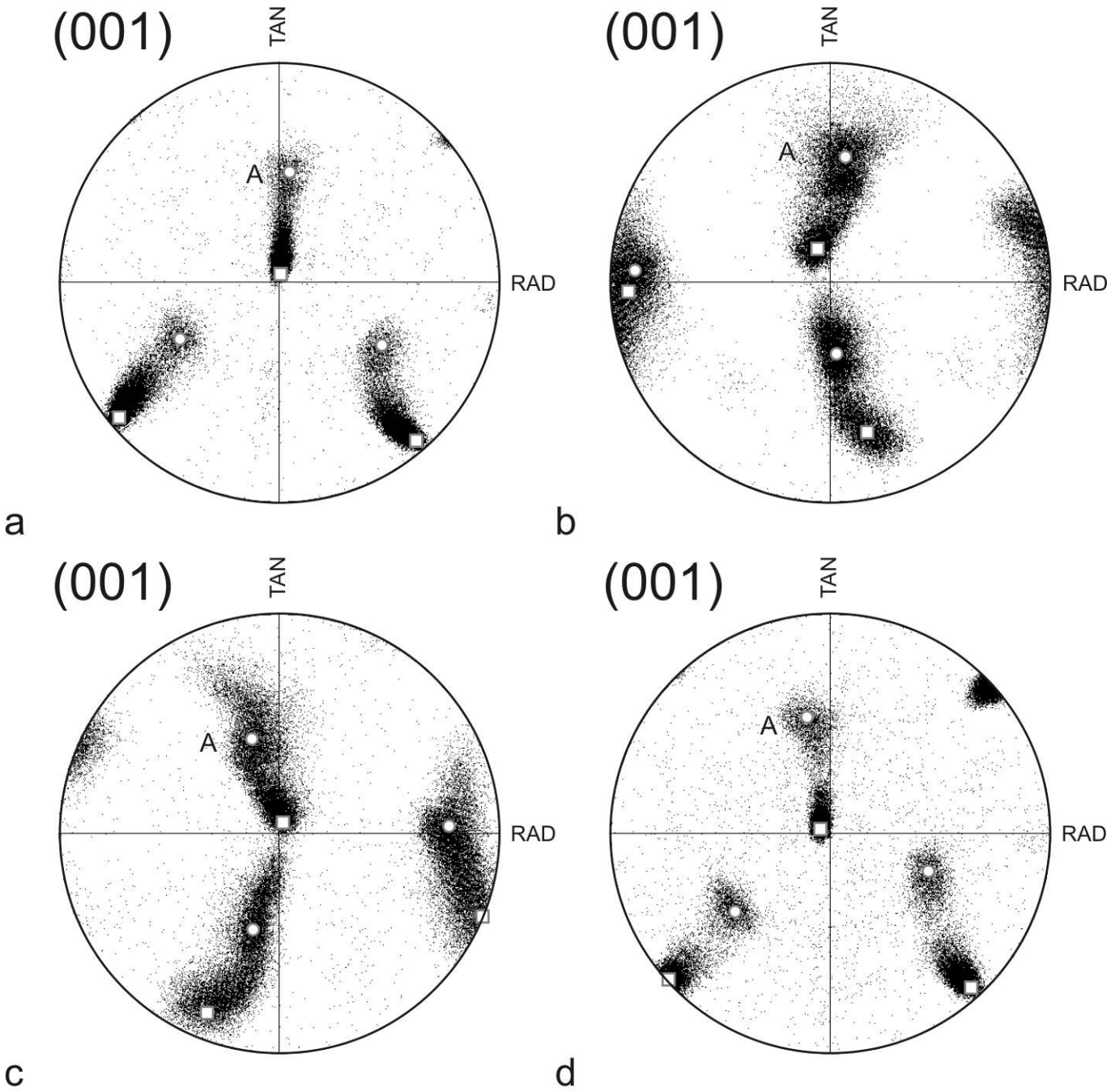

Figure 5. Tangential micro-texture scans for the <0 0 1> nickel single crystal. The maps were recorded at an equivalent strain of 1.5 and at different sample rotations of φ = (a) 0°, (b) 30°, (c) 60°, (d) 90°. The scan size of the evaluated (0 0 1) pole figures was 200μm x 200μm. In the pole figures the white squares mark the initial orientation while the white circles indicate the orientation of the regions of locally enhanced accumulated lattice rotation. The letter A marks an invariant pole about which the other white circles move

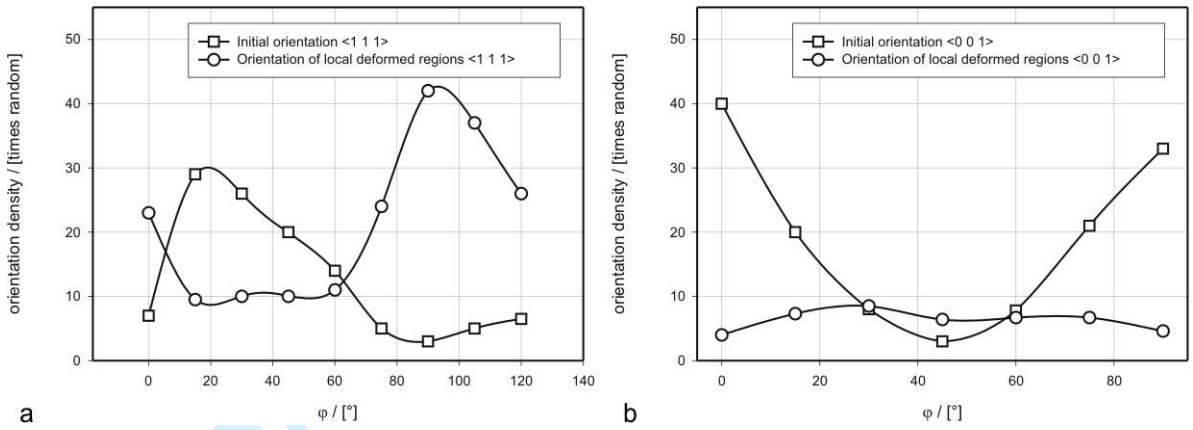

Figure 6. The density of the initial orientation is represented by square symbols and the density of the regions of locally enhanced accumulated lattice rotation is shown by circles as a function of the sample rotation φ. (a) for the <1 1 1> nickel single crystal (b) for the <0 0 1> nickel single crystal.

For Peer Review Only

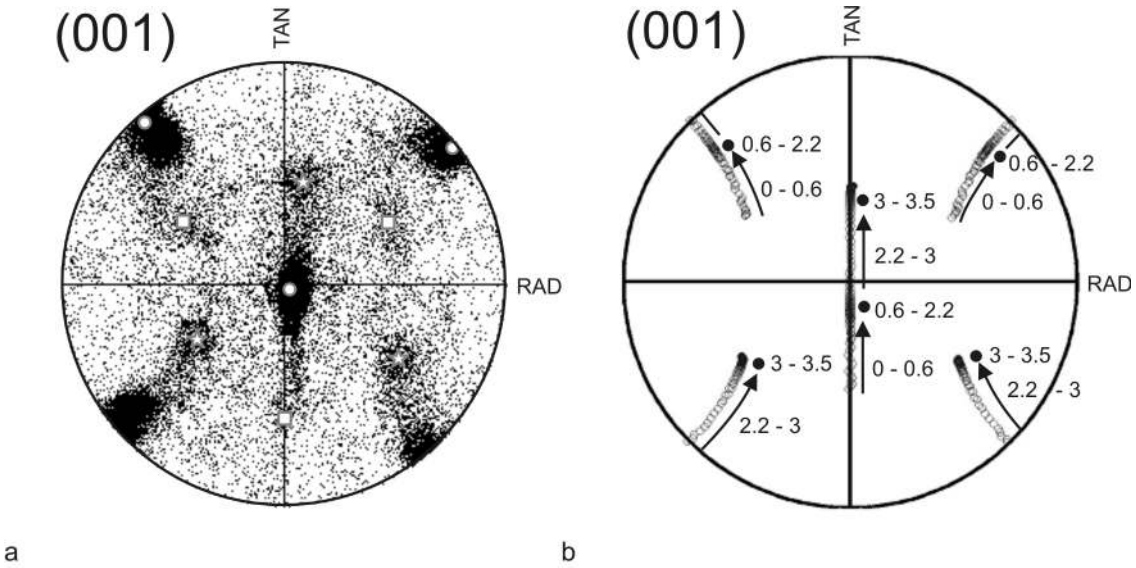

Figure 7. Comparison between a micro-texture measured for the <1 1 1> nickel single crystal, (a), and a texture simulation based on the full constrained Taylor model, (b). The white squares in (a) mark the initial orientation while the white circles indicate the first preferred orientation and the white stars refer to the second preferred orientation. In the computation, (b), a rough scale is given referring the calculated micro-texture evolution to the equivalent strain.

For Peer Review Only

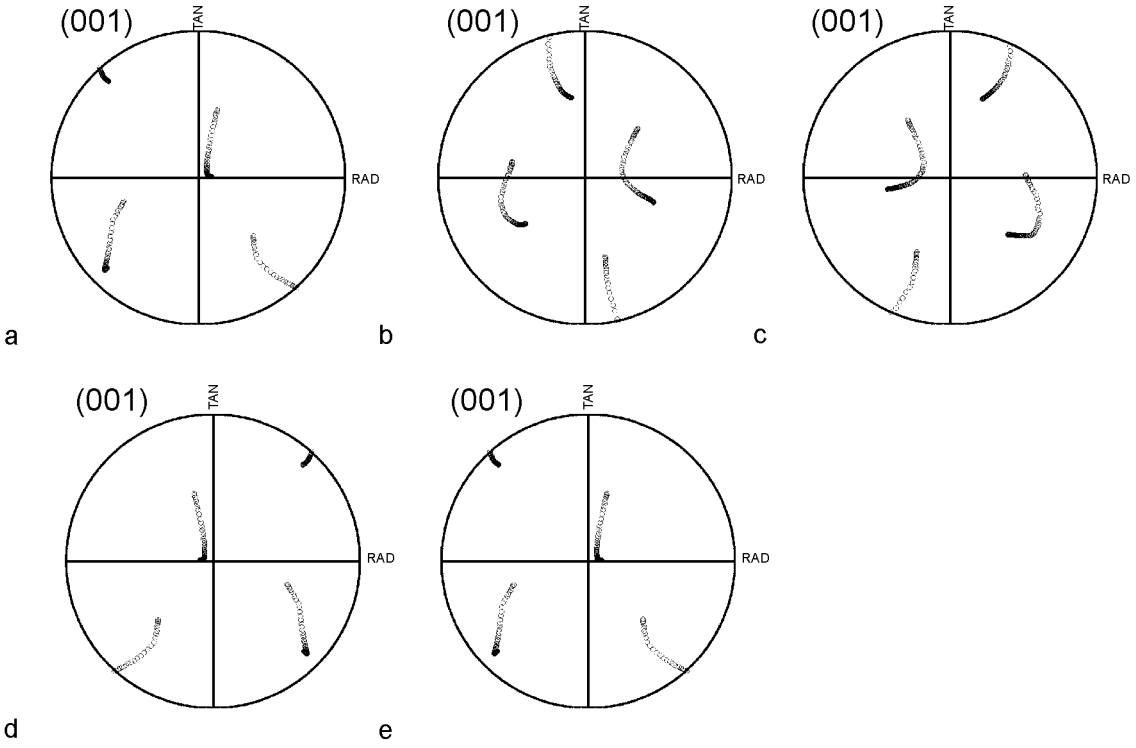

Figure 8. Numerical analysis of the texture development of the <1 1 1> orientation performed with the full constrained Taylor model for a fcc metal calculated up to $\epsilon_{eq} = 1.5$ and e = 10%. The (0 0 1) pole figures correspond to different unit cells rotated about the torsion axis by an angle of (a) 0°, (b) 30°, (c) 60°, (d) 90° and (e) 120°.

For Review Only

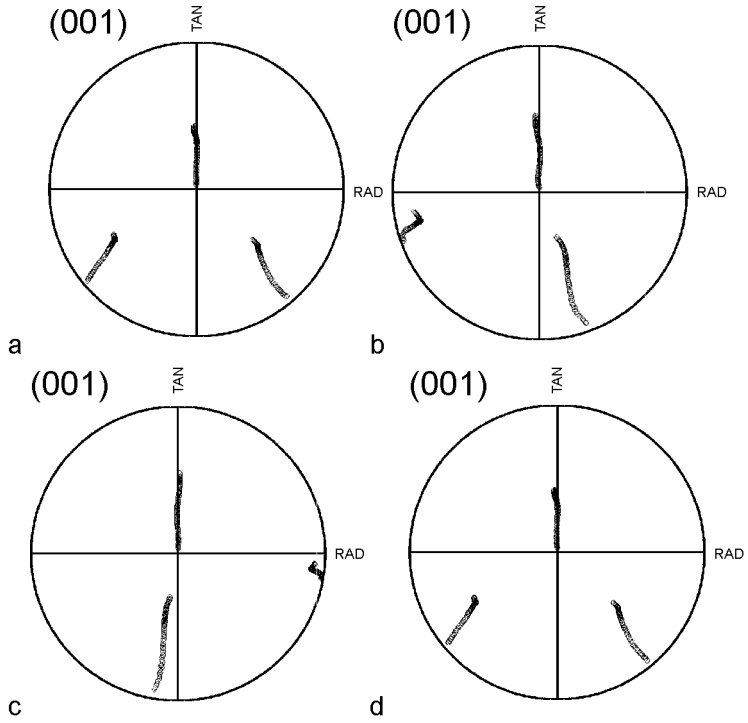

Figure 9. Results of the numerical analysis based on the full constrained Taylor model for a fcc metal calculated up to $\epsilon_{eq} = 1.5$ and e = 10%. The initial orientation was chosen in accordance with the <0 0 1> single crystal. The (0 0 1) pole figures were evaluated for sample rotations of φ = (a) 0°, (b) 30°, (c) 60°, (d) 90°.

For Peer Review Only

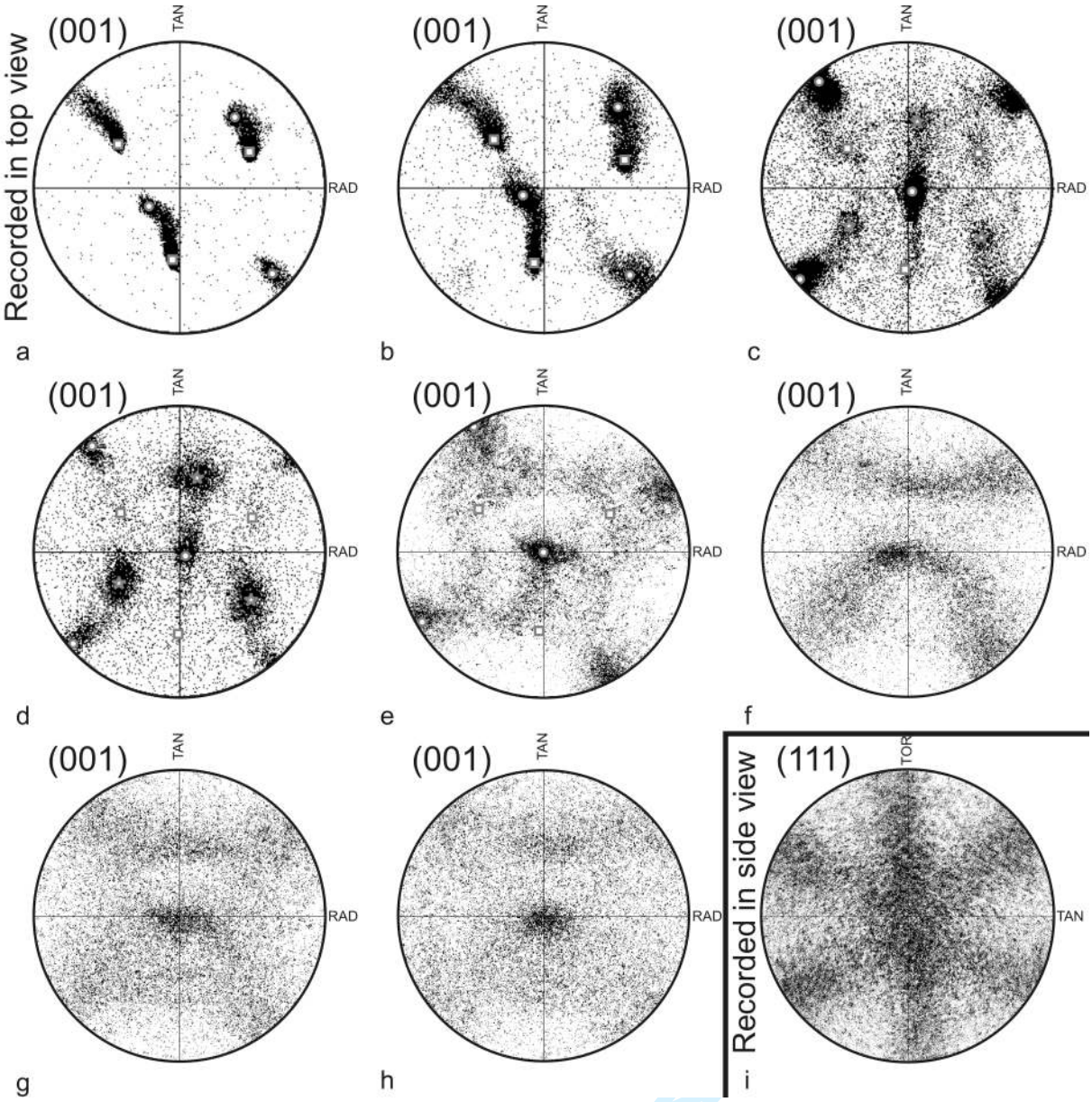

Figure 10. Texture development of the <1 1 1> nickel single crystal in the radial direction. The scan size of the evaluated pole figures was $30\mu m$ x $30\mu m$. The (0 0 1) pole figures correspond to an equivalent strain of (a) 1, (b) 2, (c) 2.5, (d) 5, (e) 8, (f) 12, (g) 16, (h) 32 and (i) 32.

For Peer Review Only

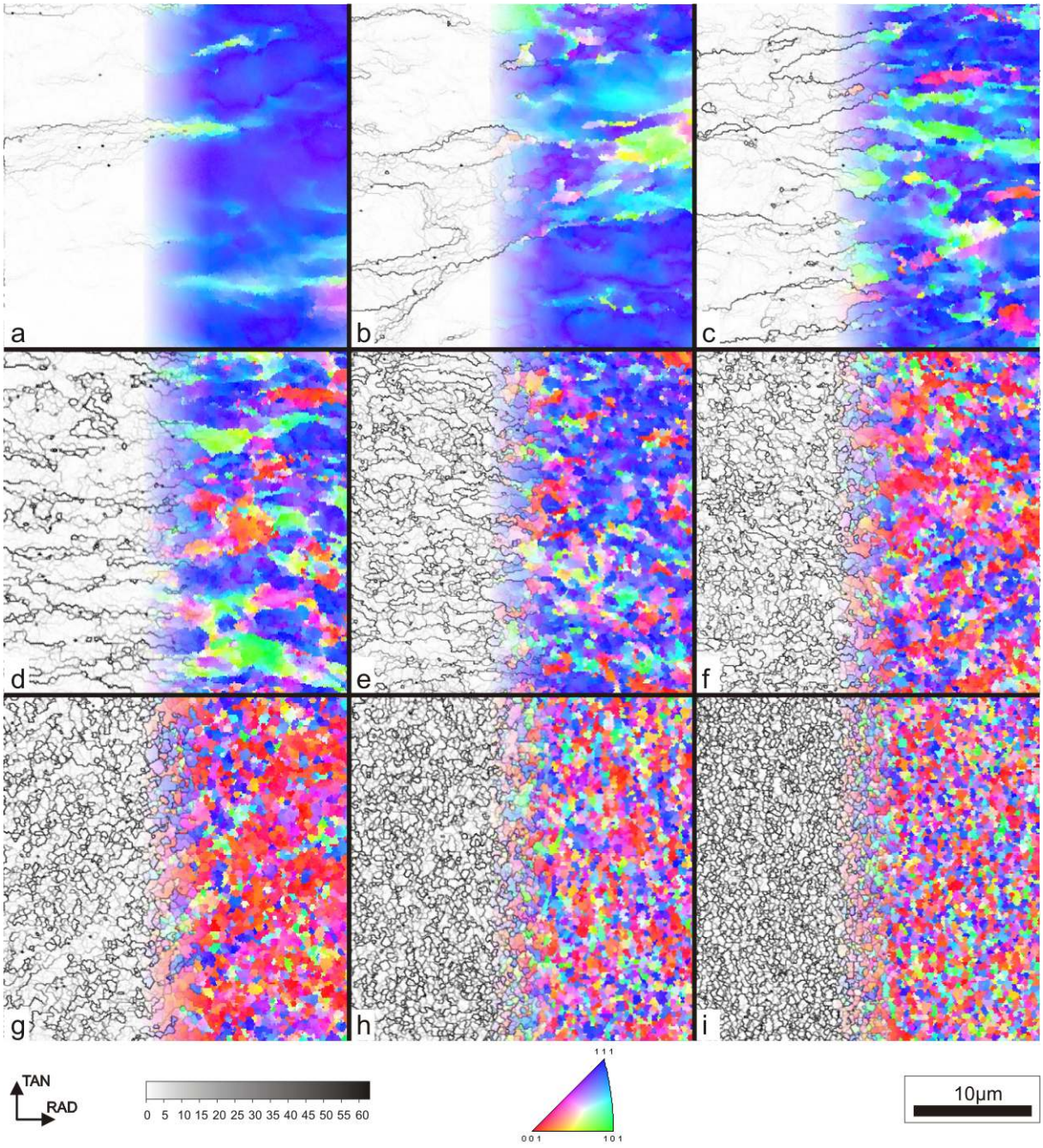

Figure 11. Structure development with increasing equivalent strain of the nickel <1 1 1> single crystal recorded in top view. The scans show the structure evolution in the radial direction with no sample rotation. The brightness of the boundaries correspond to the misorientation angle. The scans refer to the following equivalent strains (a) 1, (b) 1.5, (c) 2.25, (d) 3, (e) 4, (f) 5, (g) 8, (h) 12, (i) 32.

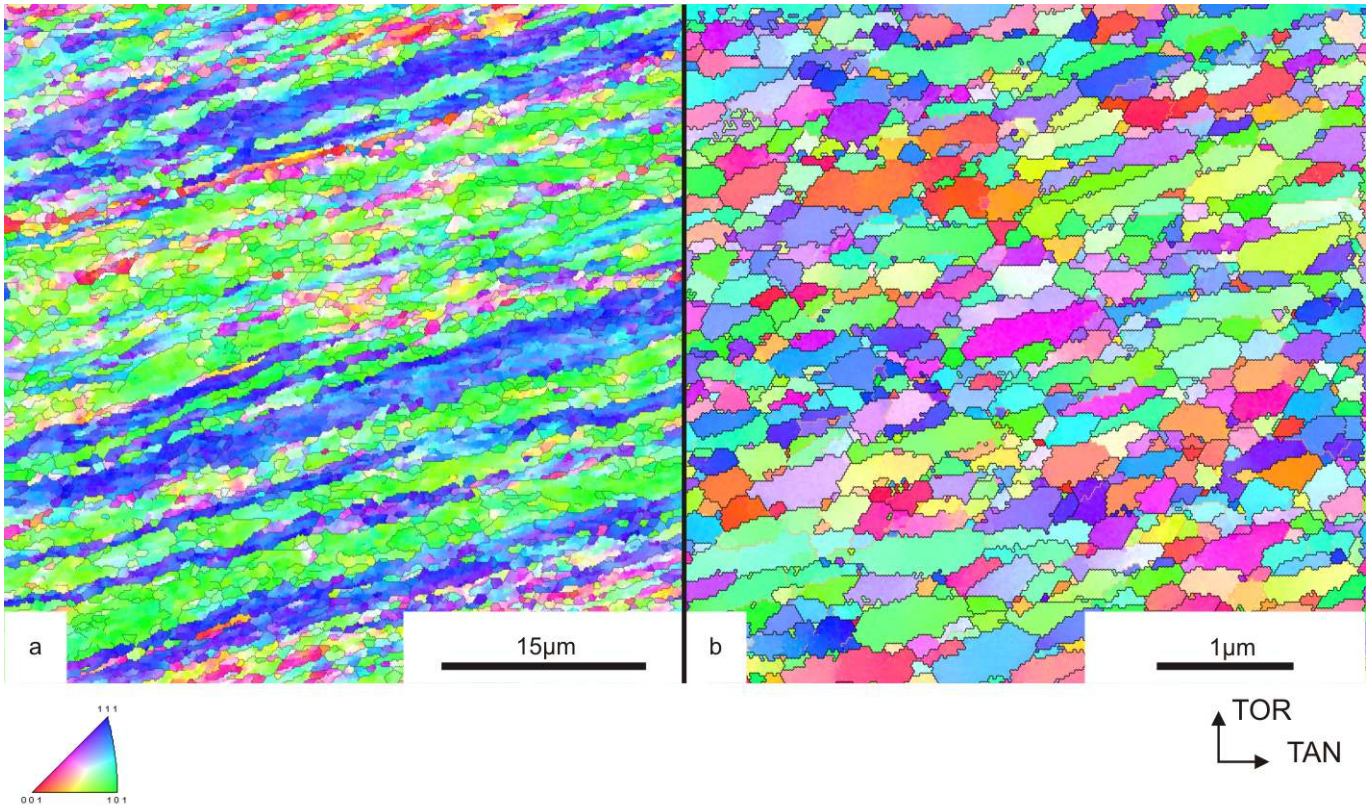

Figure 12. A comparison of the microstructure recorded in side-view of regions deformed to an equivalent strain of (a) 2.5 and (b) 32. Note the different scale bars

For Review Only

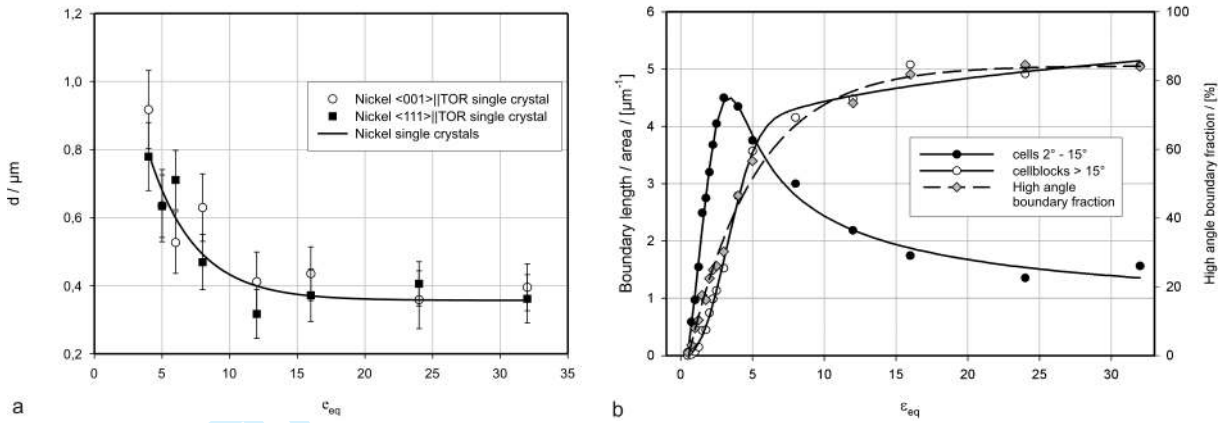

Figure 13. The decrease in structure size with increasing equivalent strain is depicted in (a) for the two single crystals with different initial crystallographic orientation. The fraction of high angle boundaries, with respect to all measured boundaries higher than 2°, is shown for the <1 1 1> nickel single crystal as a function of equivalent strain in (b).

For Peer Review Only

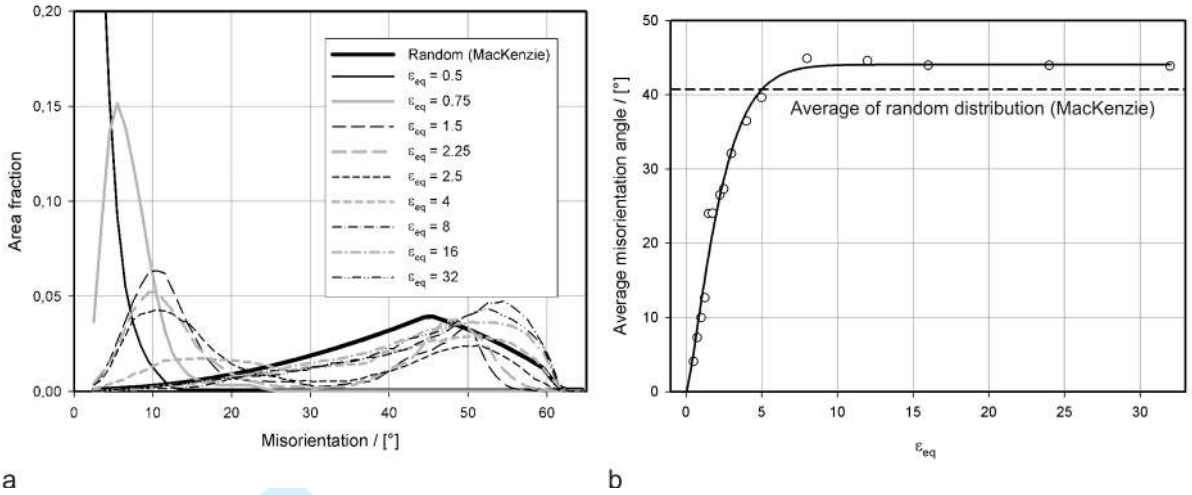

Figure 14. Misorientation distributions for different equivalent strains are shown in (a) and the average (mean) values of these distributions are plotted in (b).

For Peer Review Only

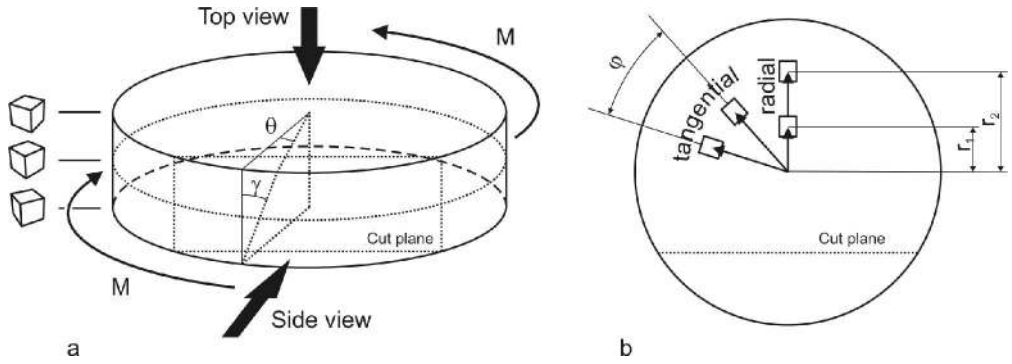

159x55mm (300 x 300 DPI)

Peer Review Only

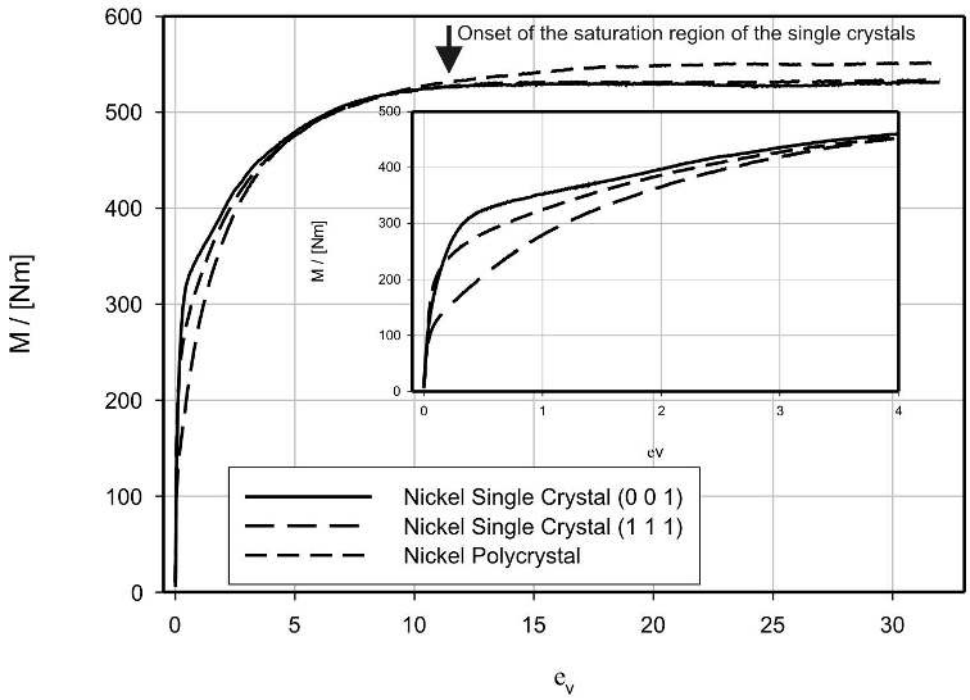

119x93mm (300 x 300 DPI)

For Review Only

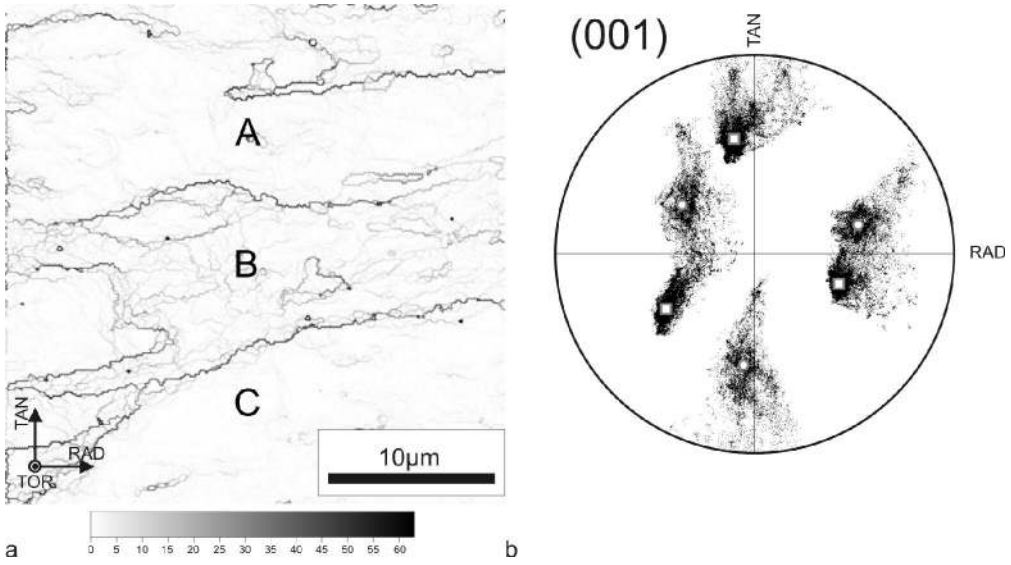

148x82mm (300 x 300 DPI)

Review Only

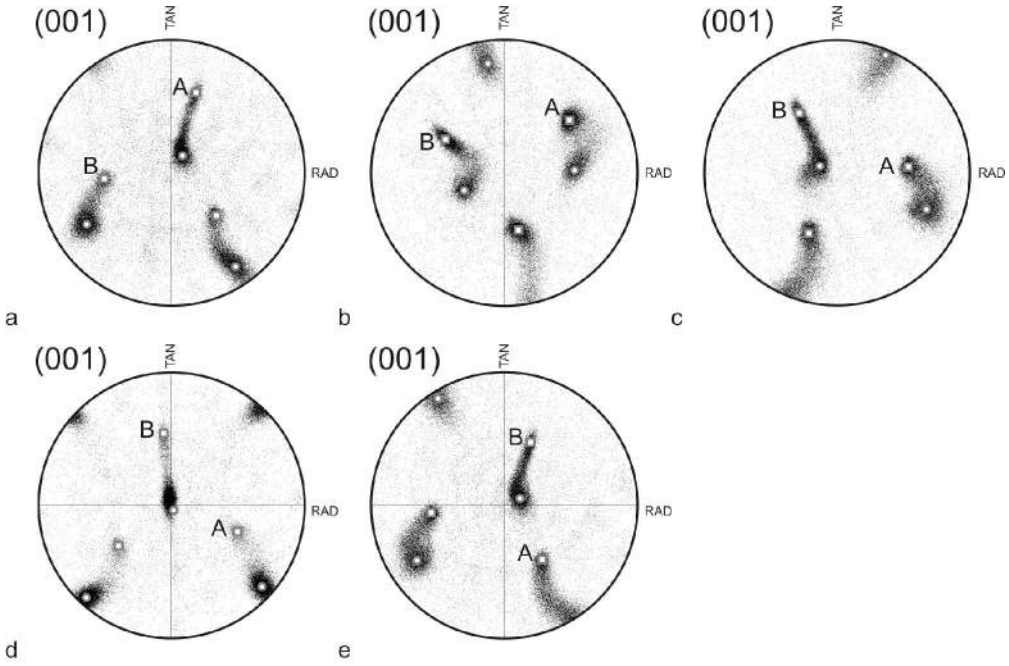

148x99mm (300 x 300 DPI)

For Review Only

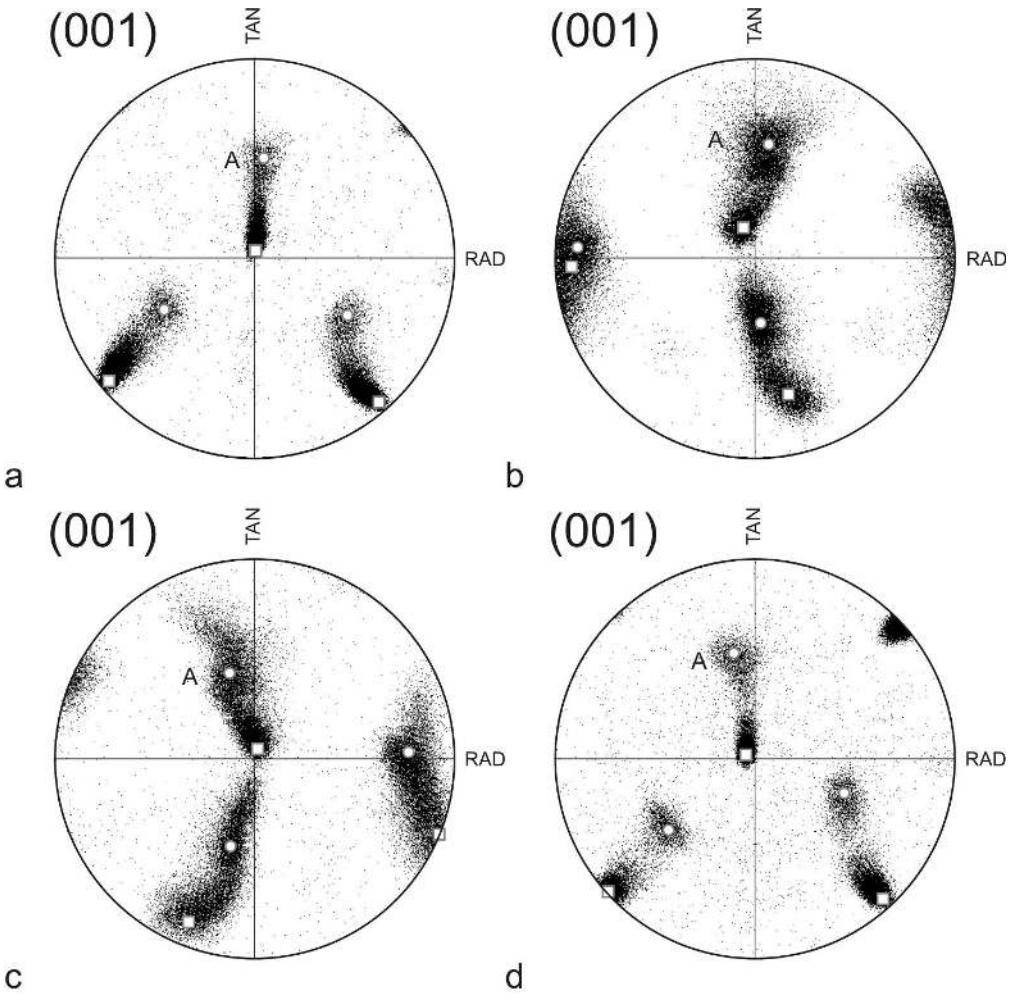

119x119mm (300 x 300 DPI)

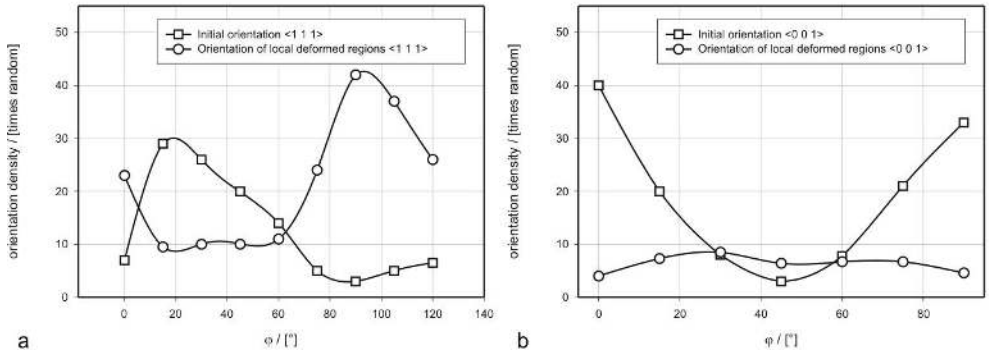

106x41mm (300 x 300 DPI)

For Peer Review Only

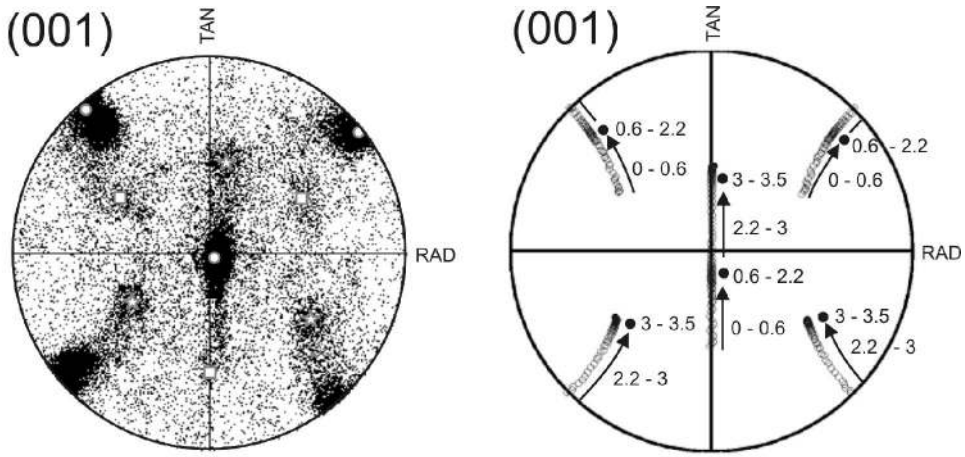

148x74mm (300 x 300 DPI)

For Review Only

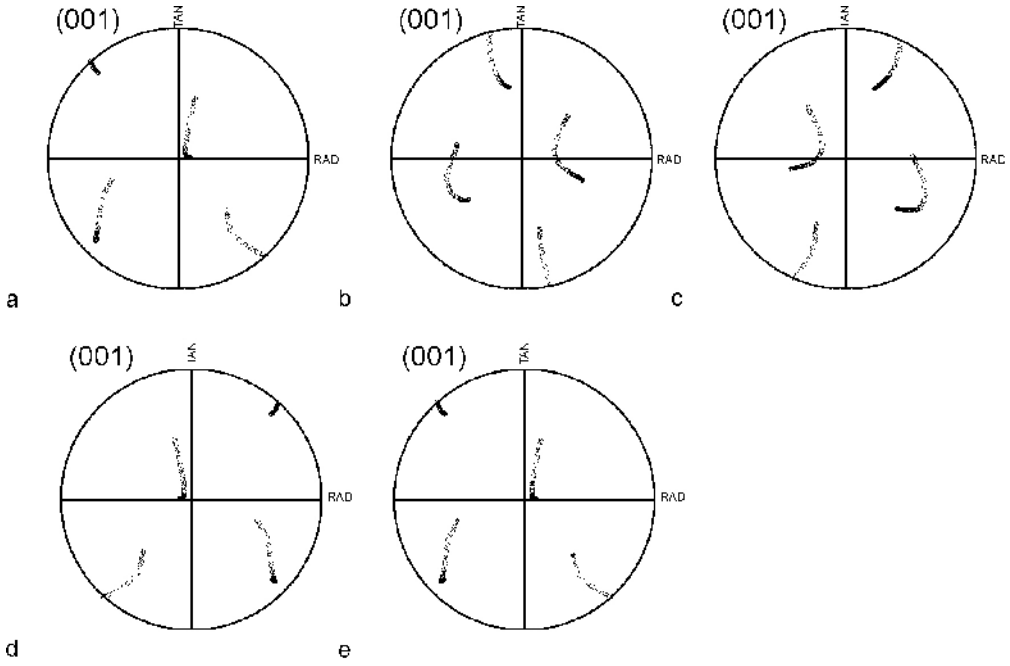

148x100mm (300 x 300 DPI)

view Only

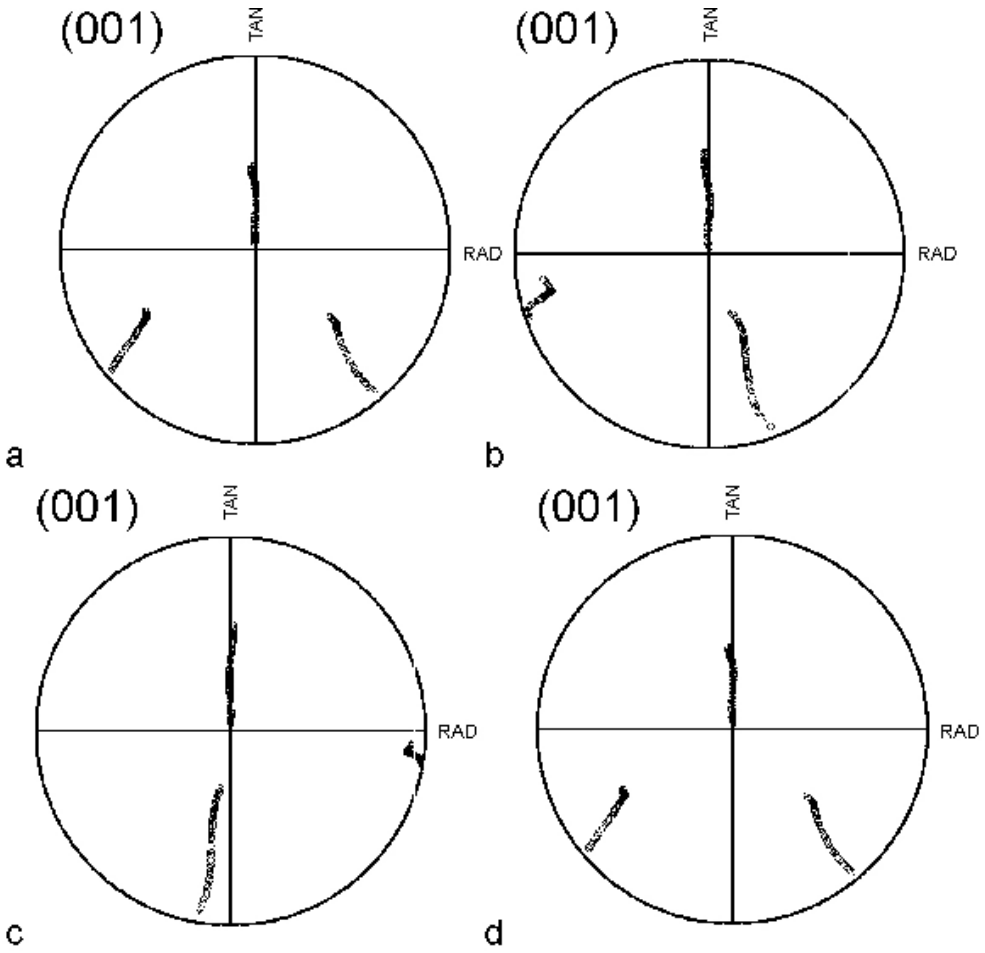

99x97mm (300 x 300 DPI)

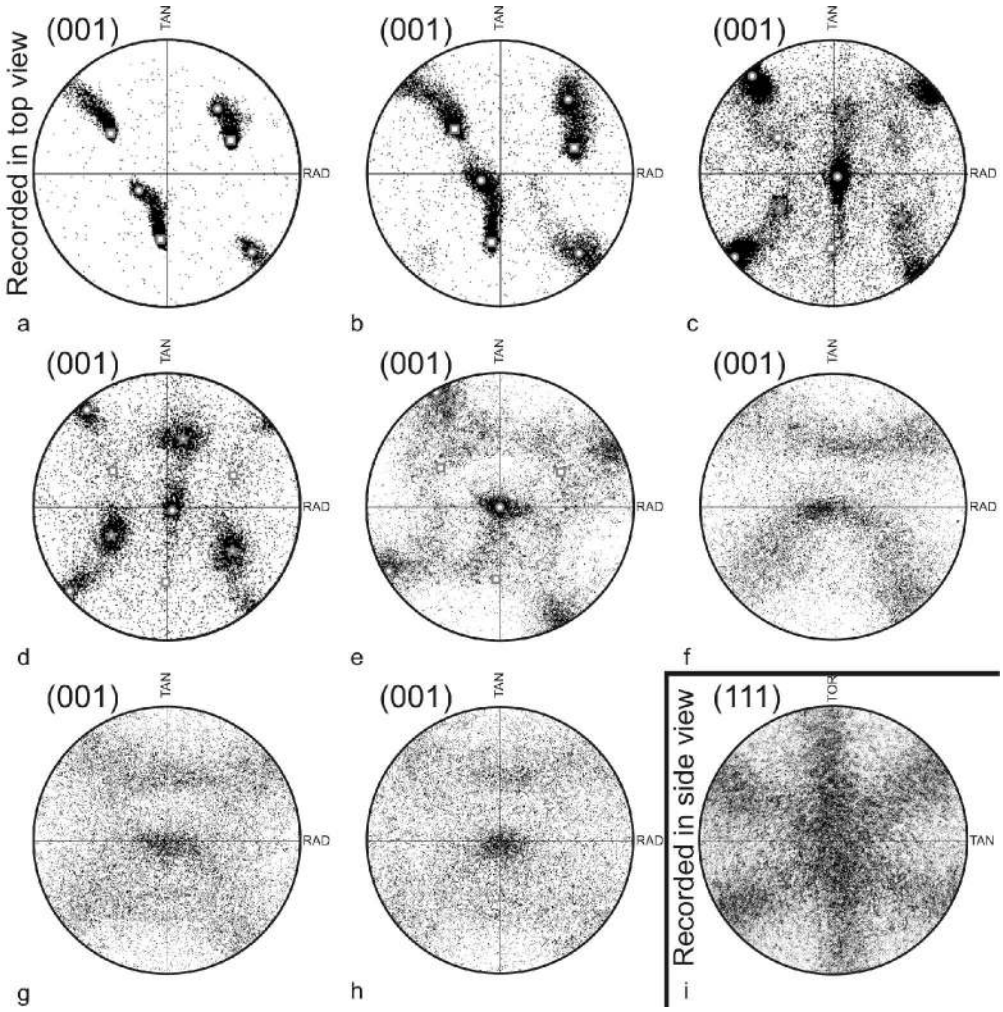

159x159mm (300 x 300 DPI)

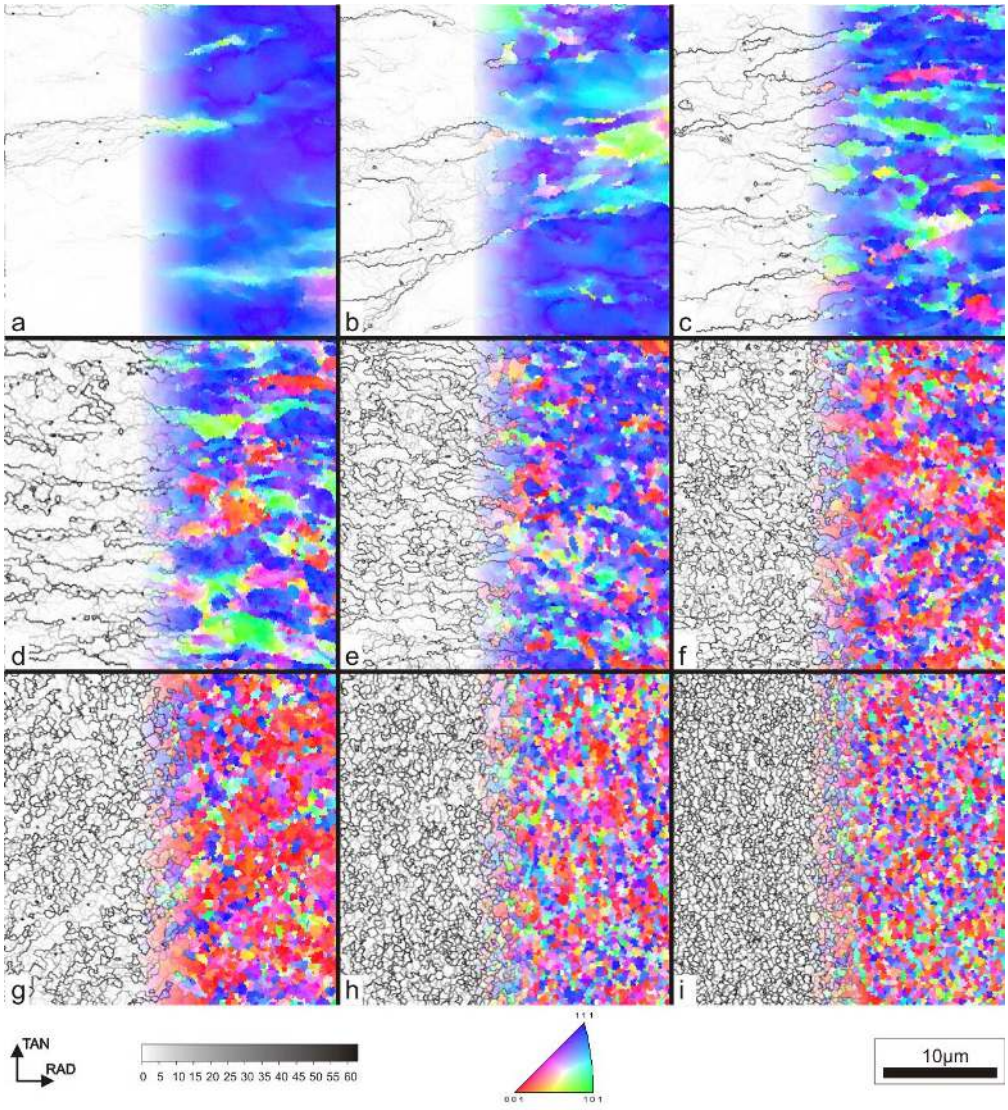

106x117mm (300 x 300 DPI)

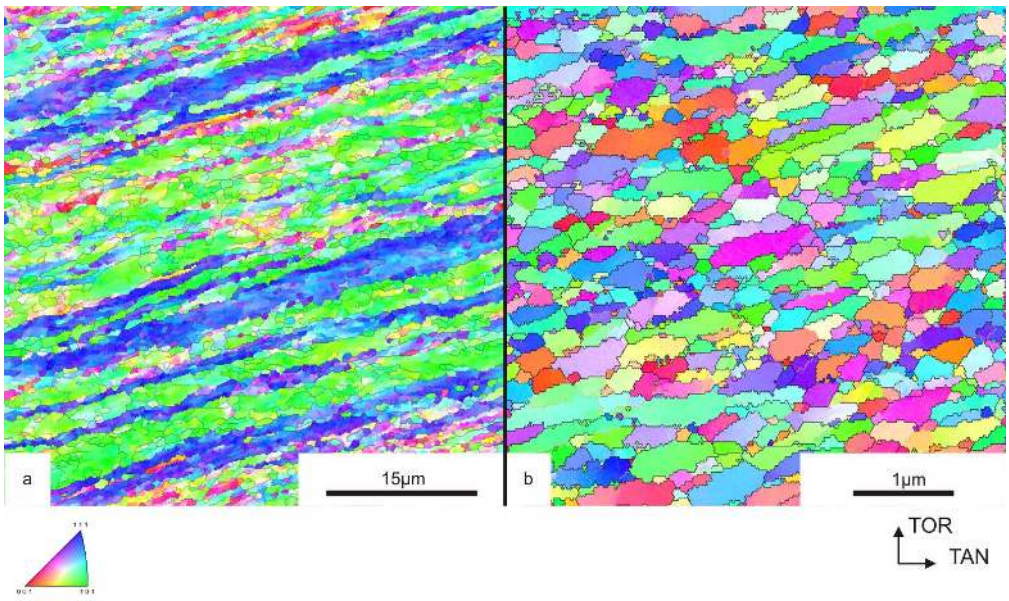

119x71mm (300 x 300 DPI)

For Review Only

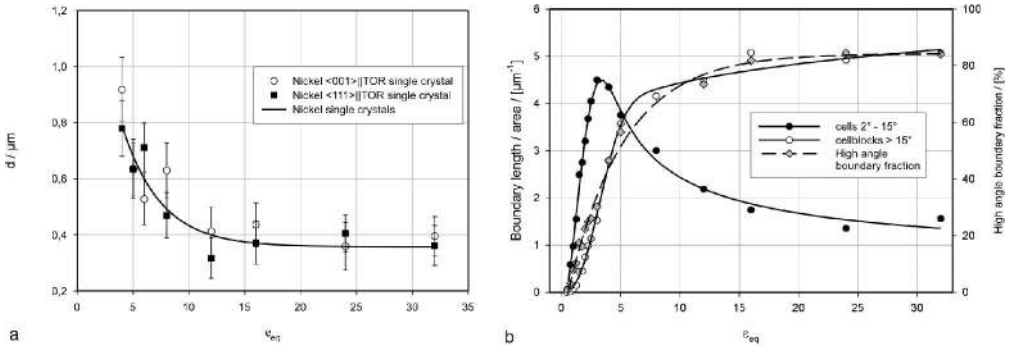

159x62mm (300 x 300 DPI)

For Peer Review Only

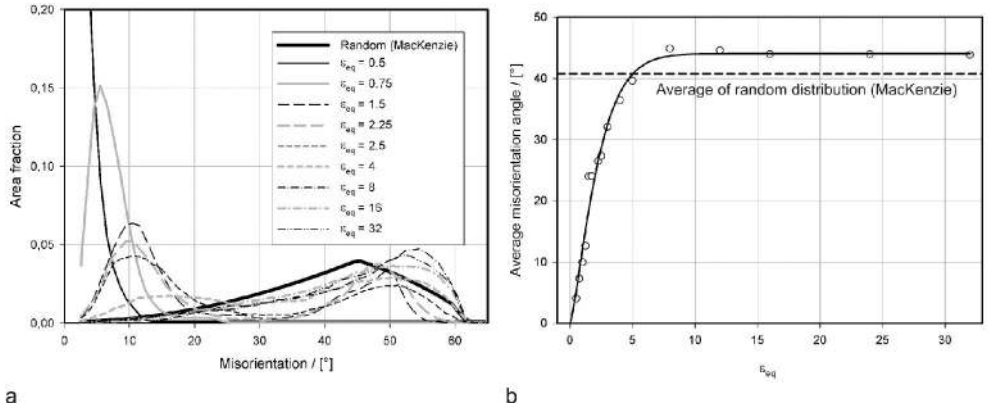

159x68mm (300 x 300 DPI)

er Review Only